

Energy loss in perturbative QCD *

R. Baier

Fakultät für Physik, Universität Bielefeld

D-33501 Bielefeld, Germany

D. Schiff

LPT, Université Paris-Sud, Bâtiment 210

F-91405 Orsay, France

B. G. Zakharov

L.D.Landau Institute for Theoretical Physics

117334 Moscow, Russia

KEYWORDS: QCD, dense nuclear matter, quark-gluon plasma, gluon radiation, energy loss,
relativistic heavy ion collisions

ABSTRACT: We review the properties of energetic parton propagation in hot or cold QCD matter, as obtained in recent works. Advances in understanding the energy loss - collisional and radiative - are summarized, with emphasis on the latter: it features very interesting properties which may help to detect the quark-gluon plasma produced in heavy ion collisions. We describe

*preprint BI-TP 2000/08, LPT-Orsay 00-22

two different theoretical approaches, which lead to the same radiated gluon energy spectrum. The case of a longitudinally expanding QCD plasma is investigated. The energy lost by a jet with given opening angle is calculated in view of making predictions for the suppression (quenching) of hard jet production. Phenomenological implications for the difference between hot and cold matter are discussed. Numerical estimates of the loss suggest that it may be significantly enhanced in hot compared to cold matter.

CONTENTS

INTRODUCTION	3
COLLISIONAL ENERGY LOSS IN QCD	4
RADIATIVE ENERGY LOSS IN QCD	7
<i>Model, basic parameters and equations</i>	8
<i>Heuristic discussion</i>	11
<i>Jet p_{\perp}-broadening</i>	14
<i>The radiative gluon energy spectrum and induced energy loss</i>	15
PATH INTEGRAL APPROACH	18
<i>Derivation of the basic formulas</i>	19
<i>Generalization to the realistic QED Lagrangian</i>	26
<i>Induced gluon emission in QCD</i>	27
<i>Comparison with the BDMPS approach</i>	29
RADIATIVE ENERGY LOSS IN AN EXPANDING QCD PLASMA	30
INDUCED ENERGY LOSS OF A HARD QUARK JET IN A FINITE CONE	33
PHENOMENOLOGICAL IMPLICATIONS	34
OUTLOOK	38
ACKNOWLEDGEMENTS	39

1 INTRODUCTION

Over the past few years, a lot of work has been devoted to the propagation of high energy partons (jets) through hot and cold QCD matter. The jet p_{\perp} -broadening and the gluon radiation induced by multiple scattering, together with the resulting radiative energy loss of the jet have been studied. These studies are extensions to QCD of the analogous QED problem considered long ago by Landau, Pomeranchuk and Migdal [1, 2]. Recent measurements [3] (reviewed in [4]) confirm the theoretical predictions in the QED case to good accuracy.

As in QED, coherent suppression of the radiation spectrum takes place when a parton propagates in a QCD medium. New and interesting predictions are found. When a high energy parton traverses a length L of hot or cold matter, the induced radiative energy loss is proportional to L^2 . The energy loss of a high energy jet in a hot QCD plasma appears to be much larger than in cold nuclear matter even at moderate temperatures of the plasma, $T \sim 200$ MeV.

The order of magnitude of the effect in hot matter compared to the case of cold nuclear matter may be expected to be large enough to lead to an observable and remarkable signal of the production of the quark-gluon plasma (QGP). Indeed, it has been proposed to measure the magnitude of “jet quenching” in the transverse momentum spectrum of hard jets produced in heavy ion collisions, noting that jet quenching is the manifestation of energy loss as seen in the suppression and change of shape of the jet spectrum compared with hadron data.

This review¹ is organized as follows: The case of elastic parton scattering giving rise to the collisional energy loss, especially in hot matter, is presented in section 2.

¹We concentrate on the more recent theoretical advances. References to earlier work are found in the quoted papers.

In section 3, we give the basic elements of the equations and describe the coherent pattern of the gluon radiative spectrum induced by multiple scattering. We derive the induced energy loss and the jet transverse momentum broadening in terms of phenomenologically significant quantities. Section 4 is devoted to the path integral approach, which provides another derivation of the induced radiative spectrum. For heavy ion collisions the case of an expanding QCD plasma is more realistic, and therefore in section 5 we consider the corresponding energy loss calculation. In section 6, we investigate the angular dependence of the radiative gluon spectrum. The dependence of the energy loss on the jet cone size is analyzed. Section 7 is devoted to estimates of the energy loss in hot QCD matter and in nuclear matter, and orders of magnitude are given. A noticeable result is that the energy loss in the case of a hot QCD medium is found to be quite collimated. Experimental indications are shortly reviewed. We close with an outlook.

2 COLLISIONAL ENERGY LOSS IN QCD

The electromagnetic energy loss of a charged particle in matter is a well studied subject [5, 6]. Similar mechanisms are responsible for the energy loss of a fast quark or gluon (jet) propagating through dense QCD matter.

In this section we discuss the loss caused by elastic collisions of the propagating quark or gluon off the (light) partons forming the dense quark-gluon plasma (QGP). In order to understand the characteristic features we consider in some detail the loss of a test quark Q traversing a plasma with quarks q and gluons g interacting elastically as $Qq \rightarrow Qq$ and $Qg \rightarrow Qg$ [7]; for a review, see [8].

The energy loss per unit length depends on the density ρ_p of the plasma con-

stituents p (with momentum k) and on the differential cross section weighted by the energy transfer $\omega = E - E'$, where $E(E')$ is the energy of the incoming (scattered) Q ,

$$-\frac{dE}{dz} = \sum_{p=q,g} \int d^3k \rho_p(k) \int dq^2 J\omega \frac{d\sigma^{Qp \rightarrow Qp}}{dq^2}. \quad (2.1)$$

J denotes the flux factor, q^2 the invariant (four) momentum transfer. Small values of q^2 dominate the collisions,

$$\frac{d\sigma^{Qp \rightarrow Qp}}{dq^2} \simeq C_p \frac{2\pi\alpha_s^2}{(q^2)^2}, \quad (2.2)$$

with $C_q = \frac{N_c^2 - 1}{2N_c^2}$, $C_g = 1$ for N_c colors. For a QGP in thermal and chemical equilibrium the densities are given by

$$\rho_q = \frac{4N_c N_f}{(2\pi)^3} n_F(k), \quad \rho_g = \frac{2(N_c^2 - 1)}{(2\pi)^3} n_B(k), \quad (2.3)$$

in terms of the Fermi-Dirac (Bose-Einstein) distributions $n_F(n_B)$. Although the factor ω in (2.1) improves the Rutherford singularity of (2.2), a logarithmic dependence still remains after the q^2 -integration, which has to be screened by medium effects, i.e. with a cut-off related to the Debye mass [9]: $-q_{\min}^2 \simeq m_D^2 = O(\alpha_s T^2)$.

Noting that $J\omega \simeq \frac{q^2}{2k}$ (when $E, E' \gg k \simeq O(T)$) one obtains [7, 8]

$$-\frac{dE}{dz} = \pi\alpha_s^2 \sum_p C_p \int \frac{d^3k}{k} \rho_p(k) \ln \frac{q_{\max}^2}{q_{\min}^2} \simeq \frac{4\pi\alpha_s^2 T^2}{3} \left(1 + \frac{N_f}{6}\right) \ln \frac{cE}{\alpha_s T}, \quad (2.4)$$

with c a numerical constant of $O(1)$, and $N_c = 3$. The strong coupling constant may be evaluated at the scale $\alpha_s(T)$ for high temperature T .

Because of the T^2 dependence of (2.4) it has been pointed out by Bjorken [7] that the collisional loss is proportional to $\sqrt{\epsilon}$, i.e. the square root of the QGP energy density, which in leading order in the coupling constant is given by $\epsilon = 8\pi^2 T^4 (1 + 21N_f/32)/15$ [10].

A proper and consistent treatment of the screening effects of the plasma in the low (soft) exchange momentum region of the collisions is indeed possible in the thermal field-theoretic framework [9], using resummed perturbation theory at high temperature. This method has been developed by Braaten and Pisarski [11, 12] and it allows one to calculate the hard thermal loop (HTL) corrections to the propagator of the exchanged gluon in the $Qq \rightarrow Qq$, and the $Qg \rightarrow Qg$ processes. The quantum field-theoretic calculation of the energy loss of a quark requires the evaluation of the discontinuity of the self-energy diagrams e.g. illustrated in Figure 1. For the soft momentum exchange (with momentum less than $q_c = O(g^{1/2}T)$) the HTL gluon propagator contributes, whereas for the hard momentum exchange ($q \simeq T$) the tree-level elastic scattering (Figure 1b) contributes [13].

The momentum cut-off q_c drops out in the sum of soft and hard contributions. It is important to note that Landau-damping effects, because of the negative q^2 values in (2.1), screen successfully the low q^2 region leading to a well defined result for dE/dz (at least to leading order in the coupling constant).

As an example the result is illustrated in Figure 2, where the energy loss of a charm quark is shown by the dashed curve using parameters characteristic for a thermalized QGP as expected in ultrarelativistic heavy ion collisions.

For light quarks the collisional energy loss for a jet propagating in a hot medium of $T = 0.25$ GeV amounts to 0.2 - 0.3 GeV/fm [8, 14], in agreement with the estimates of [7] as shown in Figure 2 (dotted curve). For a gluon jet the loss is predicted to be larger by the color factor $2N_c^2/(N_c^2 - 1) = 9/4$ than for the quark jet.

Since the QGP expected at RHIC and LHC is likely to be out of chemical

equilibrium it is necessary to investigate the energy loss in this case [15, 16]. Indeed, even away from chemical equilibrium, dynamical screening remains operational within the HTL-resummed perturbation theory. More explicitly, the collisional energy loss for a heavy quark (mass M) propagating through a QGP parametrized in terms of the distribution functions $\lambda_q n_F$ and $\lambda_g n_B$, respectively, where $\lambda_{q,g}$ are the fugacity factors describing chemical non-equilibrium, becomes

$$-\frac{dE}{dz} = 2\alpha_s \tilde{m}_g^2 \ln \left[0.920 \frac{\sqrt{ET}}{\tilde{m}_g} 2^{\lambda_q N_f / (12\lambda_g + 2\lambda_q N_f)} \right]. \quad (2.5)$$

This expression [16] is valid for energetic quarks with $E \gg M^2/T$ and contains for $\lambda_q = \lambda_g = 1$ the original result of [13]. The screening mass parameter is

$$\tilde{m}_g^2 = 4\pi\alpha_s (\lambda_g + \lambda_q N_f / 6) T^2 / 3. \quad (2.6)$$

For comparison the solid curve in Figure 2 shows the loss for the interesting case of the “early plasma phase” which is dominated by gluons ($\lambda_g = 1, \lambda_q = 0$), where the loss is exclusively due to elastic $Qg \rightarrow Qg$ scattering mediated by gluon exchange.

In summary, even when the partons propagating in hot matter have a large momentum, the collisional energy loss per unit length turns out to be less than $O(1)$ GeV/fm when reasonable values for α_s and T are taken. This estimate may be compared with the value for the hadronic string tension, $\kappa \simeq 1$ GeV/fm, which measures the slowing down of a high momentum quark in (cold) nuclear matter [17].

3 RADIATIVE ENERGY LOSS IN QCD

3.1 Model, basic parameters and equations

We imagine a very energetic quark of energy E propagating through a QCD medium of finite length L . Multiple scattering of this projectile in the medium induces gluon radiation, which gives rise to the quark energy loss.

The main assumption [18, 19] is that the scattering centers are static and uncorrelated (in the spirit of the Glauber picture). We thus focus on purely radiative processes since the collisional energy loss vanishes in the case of static centers.

We define a normalized quark-“particle” cross-section

$$V(Q^2) = \frac{1}{\pi\sigma} \frac{d\sigma}{dQ^2}, \quad (3.7)$$

where Q is the 2-dimensional transverse momentum transfer scaled by an appropriate scale :

$$\begin{aligned} \vec{Q} &= \frac{\vec{q}}{\mu}, \\ \text{and} \quad \sigma &= \int \frac{d\sigma}{d^2Q} d\vec{Q} \quad . \end{aligned} \quad (3.8)$$

In the case of a hot QCD plasma, the “particle” is a quark or gluon and it is a nucleon in the case of cold matter. $d\sigma/d^2Q$ depends only on \vec{Q} , as it is usually assumed for diffractive kinematics with very large incident energy. The scale μ characteristic of the medium is conveniently taken as the Debye screening mass in the hot case and as a typical momentum transfer in a quark-nucleon collision. The condition that the independent scattering picture be valid may be expressed as :

$$\mu^{-1} \ll \lambda, \quad (3.9)$$

where λ is the parton mean free path in the medium $\lambda = 1/\rho\sigma$, and ρ is the density of the medium. We assume that a large number of scatterings takes

place, that is

$$L \gg \lambda. \quad (3.10)$$

Successive scatterings being independent, the parton propagation is "time-ordered" and time-ordered perturbation theory is the natural framework to calculate the radiation amplitude. Let us give a sketch of the basic equations, referring the reader to [20, 21] for further details. We may number the scattering centers depending on the interaction time and write for the radiation spectrum induced by N scatterings

$$\omega \frac{dI}{d\omega} = \frac{\alpha_s}{2\pi^2} \int d\vec{k}_\perp \left\langle \sum_{i=1}^N \sum_{j=1}^N \vec{J}_{eff}^i \cdot \vec{J}_{eff}^{j\dagger} e^{i(\varphi_i - \varphi_j)} \right\rangle, \quad (3.11)$$

where \vec{J}_{eff}^i is an effective current for the gluon emission induced by center i . It includes color factors consistent with the overall normalization to the elastic scattering cross section. The phase φ_i is associated to time t_i (longitudinal coordinate z_i) by $\varphi_i = t_i k_\perp^2 / \omega$.

The brackets indicate averaging - over momentum transfers and over z_i - for which a simplified model is

$$\langle (\dots) \rangle \Leftrightarrow \int \prod_{\ell=1}^{N-1} \frac{d\Delta_\ell}{\lambda} \exp\left(-\frac{\Delta_\ell}{\lambda}\right) \cdot \int \prod_{i=1}^N d\vec{q}_{i\perp} V(q_{i\perp}^2) (\dots), \quad (3.12)$$

where $\Delta_\ell = z_{\ell+1} - z_\ell$. We rewrite (3.11) as

$$\omega \frac{dI}{d\omega} = \frac{\alpha_s}{2\pi^2} \int d\vec{k}_\perp \cdot \left\langle 2 \operatorname{Re} \sum_{i=1}^N \sum_{j=i+1}^N \vec{J}_{eff}^i \cdot \vec{J}_{eff}^{j\dagger} \left(e^{i(\varphi_i - \varphi_j)} - 1 \right) + \left| \sum_{i=1}^N \vec{J}_{eff}^i \right|^2 \right\rangle, \quad (3.13)$$

which allows one to exhibit the so-called factorization contribution: the second term in (3.13) which corresponds to the limit of vanishing phases. This contribution is equivalent to the radiation spectrum induced by a single scattering of momentum transfer $\vec{q}_{\perp tot} = \sum_{i=1}^N \vec{q}_i$. It has at most a weak logarithmic medium

dependence [21]. We concentrate in the following on the medium-induced radiation spectrum and drop the factorization term. In the limit of large- N_c and replacing sums over i and j by integrals, i.e. taking the sum over scatterings to be arbitrary in number, the following expression for the spectrum per unit length of the medium is obtained,

$$\omega \frac{dI}{d\omega dz} = \frac{\alpha_s N_c}{2\pi^2 L} \int_0^L d\Delta \int_0^{L-\Delta} \frac{dz_1}{\lambda} \int d\vec{U} \cdot \left\langle 2\text{Re} \sum_{n=0}^{\infty} \vec{J}_1 \cdot \vec{J}_{n+2} \left[\exp \left\{ i\kappa \sum_{\ell=1}^{n+1} U_\ell^2 \frac{\Delta_\ell}{\lambda} \right\} - 1 \right] \delta \left(\Delta - \sum_{m=1}^{n+1} \Delta_m \right) \right\rangle, \quad (3.14)$$

with $\vec{U} = \vec{k}_\perp/\mu$ and $\kappa = \lambda\mu^2/2\omega$. In the soft gluon limit the rescaled emission current is given by

$$\vec{J}_i = \left(\frac{\vec{U}_i}{U_i^2} - \frac{\vec{U}_i + \vec{Q}_i}{(\vec{U}_i + \vec{Q}_i)^2} \right). \quad (3.15)$$

Eq. (3.14) exhibits the interference nature and coherent pattern of the spectrum. The phase factor as it appears here may be understood in terms of formation time arguments which will be discussed heuristically in the next section. It can be shown moreover [21] that (3.14) leads to a simple structure of the spectrum per unit length which will be the starting point of section 3.4:

$$\omega \frac{dI}{d\omega dz} = \frac{\alpha_s N_c}{\pi^2 L} \text{Re} \int_0^L \frac{d\Delta}{\lambda} \int_0^{L-\Delta} \frac{dz_1}{\lambda} \int d\vec{U} \vec{f}(\vec{U}, \Delta) \cdot \vec{f}_{Born}(\vec{U}) \Big|_{\kappa}^{\kappa=0}, \quad (3.16)$$

where $\vec{f}_{Born}(\vec{U})$ is the Born amplitude defined as

$$\vec{f}_{Born}(\vec{U}) = \int d\vec{Q}_1 V(Q_1^2) \vec{J}_1, \quad (3.17)$$

and $\vec{f}(\vec{U}, \Delta)$ is the evolved amplitude which satisfies a Bethe-Salpeter type equation. Subtracting in (3.16) the contribution for $\kappa = 0$ corresponds in (3.14) to subtracting the zero phase contribution. The generic structure of (3.16) is illustrated in Figure 3. The reader may question the one-gluon exchange approximation as shown in this Figure 3. In fact, the scale of the coupling for each

individual scattering is set by the accumulated overall transverse momentum.

This justifies the perturbative treatment.

3.2 Heuristic discussion

In the following discussion we neglect logarithmic and numerical factors of $O(1)$, but keep all relevant parameters.

The semi-quantitative argument which allows one to understand the coherent pattern of the induced gluon radiation is the following. One defines the formation time of the radiation,

$$t_{\text{form}} \simeq \frac{\omega}{k_{\perp}^2}, \quad (3.18)$$

where ω and k_{\perp} are the gluon energy and transverse momentum (with $\omega \gg k_{\perp}$ and the typical $k_{\perp} \simeq \mu$). When $t_{\text{form}} \gg \lambda$, radiation takes place in a coherent fashion with many scattering centers acting as a single one. Let us introduce the coherence time (length) l_{coh} which plays an important role in the following considerations. It is associated with the formation time of a gluon radiated by a group of scattering centers which acts as one source of radiation,

$$l_{\text{coh}} \simeq \frac{\omega}{\langle k_{\perp}^2 \rangle_{l_{\text{coh}}}}, \quad (3.19)$$

with

$$\langle k_{\perp}^2 \rangle_{l_{\text{coh}}} \simeq \frac{l_{\text{coh}}}{\lambda} \mu^2 \equiv N_{\text{coh}} \mu^2, \quad (3.20)$$

assuming a random walk expression for the accumulated gluon transverse momentum. One derives the estimate

$$l_{\text{coh}} \simeq \sqrt{\frac{\lambda}{\mu^2}} \omega, \quad (3.21)$$

so that the number of coherent scatterings becomes

$$N_{\text{coh}} \simeq \sqrt{\frac{\omega}{\lambda \mu^2}} \equiv \sqrt{\frac{\omega}{E_{\text{LPM}}}}, \quad (3.22)$$

where the energy parameter $E_{\text{LPM}} \equiv \lambda\mu^2$ is introduced [22], in analogy with the QED Landau-Pomeranchuk-Migdal (LPM) phenomenon.

For small $\omega \leq E_{\text{LPM}}$, incoherent radiation takes place on L/λ scattering centers. Using the soft ω limit for the single scattering spectrum [23]

$$\frac{\omega dI}{d\omega} \simeq \frac{\alpha_s}{\pi} N_c, \quad (3.23)$$

the differential energy spectrum per unit length in the so-called Bethe-Heitler (BH) regime for incoherent radiation is derived,

$$\left. \frac{\omega dI}{d\omega dz} \right|_{\text{BH}} = \frac{1}{L} \left. \frac{\omega dI}{d\omega} \right|_L \simeq \frac{\alpha_s}{\pi} N_c \frac{1}{\lambda}, \quad (3.24)$$

with $l_{\text{coh}} \leq \lambda$ and $\omega \leq \omega_{\text{BH}} \equiv E_{\text{LPM}}$.

The interesting regime of coherent radiation (LPM regime) is defined by $\lambda < l_{\text{coh}} < L$ ($N_{\text{coh}} > 1$), i.e.

$$E_{\text{LPM}} = \omega_{\text{BH}} < \omega < \min\{\omega_{\text{fact}}, E\}, \quad (3.25)$$

with $\omega_{\text{fact}} \sim \frac{\mu^2}{\lambda} L^2$. Since the N_{coh} groups are acting as effective single scattering centers the energy spectrum is estimated as

$$\left. \frac{\omega dI}{d\omega dz} \right|_{\text{LPM}} \simeq \frac{1}{l_{\text{coh}}} \left. \frac{\omega dI}{d\omega} \right|_{l_{\text{coh}}} \simeq \frac{\alpha_s}{\pi} N_c \frac{1}{l_{\text{coh}}} \simeq \frac{\alpha_s}{\pi} N_c \sqrt{\frac{\mu^2}{\lambda} \frac{1}{\omega}}. \quad (3.26)$$

Comparing (3.26) with (3.24) we find a suppression factor given by $\sqrt{E_{\text{LPM}}/\omega}$.

For $l_{\text{coh}} \geq L$, i.e. when

$$\omega > \omega_{\text{fact}} = E_{\text{LPM}} \left(\frac{L}{\lambda} \right)^2, \quad (3.27)$$

effectively only one scattering is active (factorization regime), and correspondingly for $\omega_{\text{fact}} < \omega < E$,

$$\left. \frac{\omega dI}{d\omega dz} \right|_{\text{fact}} \simeq \frac{\alpha_s}{\pi} N_c \frac{1}{L}. \quad (3.28)$$

The expressions for the spectrum per unit length in the different regimes (Eqs.(3.24), (3.26) and (3.28)) hold for a medium of finite length $L < L_{cr}$, where

$$L_{cr} = \lambda \sqrt{E/E_{LPM}}, \quad (3.29)$$

as derived from the condition that $\omega_{\text{fact}} \leq E$ (correspondingly, the condition $E > E_{cr} = E_{LPM}(L/\lambda)^2$ has to be satisfied). A discussion of the radiation spectrum can be found in [21].

In order to obtain the energy loss per unit distance $-dE/dz$ one integrates the gluon spectrum over ω , with $0 \leq \omega \leq E$. In addition to a medium independent contribution proportional to $\frac{\alpha_s}{\pi} N_c \frac{E}{L}$ (the factorization contribution), we obtain from (3.26) the medium induced (LPM) loss, proportional to the size of the medium and given by

$$-dE/dz \simeq \frac{\alpha_s}{\pi} N_c \sqrt{\frac{\mu^2}{\lambda} \omega_{\text{fact}}} \simeq \frac{\alpha_s}{\pi} N_c \frac{\mu^2}{\lambda} L, \quad (3.30)$$

for $L < L_{cr}$. Integrating over z leads to the total loss growing as L^2 . For $L > L_{cr}$ (i.e. $E < E_{cr}$), the size does not affect the loss per unit length,

$$-dE/dz \simeq \frac{\alpha_s}{\pi} N_c \sqrt{\frac{\mu^2}{\lambda} E} = \frac{\alpha_s}{\pi} \frac{N_c}{\lambda} \sqrt{E_{LPM} E}, \quad (3.31)$$

i.e. a dependence proportional to \sqrt{E} is obtained, which is familiar from the QED-coherent LPM suppression [1].

In Figure 4 the energy loss

$$-\Delta E \equiv \int_0^L -\frac{dE}{dz} dz, \quad (3.32)$$

for the induced and the factorization cases, is shown as a function of L (N_c is taken to be 1).

Using the random walk expression for the accumulated transverse momentum

of the gluon due to successive scatterings in the medium of size L ,

$$\langle k_{\perp}^2 \rangle_L \simeq \mu^2 L/\lambda, \quad (3.33)$$

and inserting this relation in (3.30), one obtains

$$-dE/dz \simeq \frac{\alpha_s}{\pi} N_c \langle k_{\perp}^2 \rangle_L, \quad (3.34)$$

a relation between the induced energy loss and the jet broadening, which is independent of the details of the interaction.

3.3 Jet p_{\perp} -broadening

On the way to deriving the gluon radiative spectrum, let us start with the classical diffusion equation satisfied by the transverse momentum distribution of a high energy parton which encounters multiple scattering in a medium. Suppose the parton is produced in a hard collision with an initial transverse momentum distribution $f_0(U^2)$; U is the dimensionless transverse momentum $\vec{U} \equiv \vec{p}/\mu$ and $\int d\vec{U} f_0(U^2) = 1$.

Neglecting the transverse momentum given to the parton by induced gluon emission, one can derive a kinetic equation for the transverse momentum distribution $f(U^2, z)$ after a distance z in the medium [24].

In terms of the variable $t = z/\lambda_R$ with λ_R the mean free path for a parton of color representation R , one finds the following gain-loss equation

$$\begin{aligned} \frac{\partial f(U^2, t)}{\partial t} = & + \int f(U'^2, t) V((\vec{U}' - \vec{U})^2) d\vec{U}' \\ & - \int f(U^2, t) V((\vec{U} - \vec{U}')^2) d\vec{U}', \end{aligned} \quad (3.35)$$

with

$$f(U^2, 0) = f_0(U^2). \quad (3.36)$$

Defining $\tilde{f}(B^2, t)$ as

$$\tilde{f}(B^2, t) = \int d\vec{U} e^{-i\vec{B}\cdot\vec{U}} f(U^2, t), \quad (3.37)$$

and

$$\tilde{V}(B^2) = \int d\vec{Q} e^{-i\vec{B}\cdot\vec{Q}} V(Q^2), \quad (3.38)$$

we find

$$\frac{\partial \tilde{f}(B^2, t)}{\partial t} = -\frac{1}{4} B^2 \tilde{v}(B^2) \tilde{f}(B^2, t), \quad (3.39)$$

with

$$\tilde{v}(B^2) \equiv \frac{4}{B^2} (1 - \tilde{V}(B^2)). \quad (3.40)$$

It is possible to define a characteristic width of the distributions $f(U^2, t)$ which is found to be [24]:

$$p_{\perp W}^2 = \frac{\mu^2}{\lambda_R} L \tilde{v}(\lambda_R/L). \quad (3.41)$$

The linear growth with L is expected and is used to discuss p_{\perp} -broadening of high energy partons in nuclei. The coefficient $\hat{q} = \frac{\mu^2}{\lambda} \tilde{v}$ plays the role of a transport coefficient as encountered in diffusion equations. (3.41) is valid for hot and cold QCD media.

3.4 The radiative gluon energy spectrum and induced energy loss

Let us now turn to the gluon spectrum ². We shall concentrate on a quark jet. The general case is given in [25]. As sketched in section 3.1 and derived in [20, 21, 25], the spectrum for the radiated gluon is calculated in terms of the interference term between the quark-gluon amplitude at time t and the complex conjugate Born amplitude. For simplicity, we restrict ourselves here to the case where the quark enters the medium from outside. (An additional term is needed

²For related discussions of gluon bremsstrahlung in dense matter see also [26, 27]

in the case when the quark is produced via a hard scattering at $t = 0$ in the medium). We denote by $f(\vec{U}, \vec{V}, t)$ the quark gluon amplitude at time t . \vec{U} is the scaled gluon momentum $\vec{U} \equiv \frac{\vec{k}}{\mu}$ and $\vec{V} - \vec{U}$ the scaled quark momentum as illustrated in Figure 5.

To account for the gluon polarization, f is a 2-dimensional vector which will be implied hereafter. The dependence on \vec{U} and \vec{V} is actually only in the combination $\vec{U} - x\vec{V}$ with $x = k/p$. The amplitude $f(\vec{U}, \vec{V}, t)$ satisfies the initial condition $f(\vec{U}, \vec{V}, 0) = f_{Born}(\vec{U}, \vec{V})$, where f_{Born} is the Born amplitude to be described shortly.

The induced gluon spectrum is written as :

$$\frac{\omega}{d\omega} \frac{dI}{dz} = \frac{\alpha_s C_F}{\pi^2 L} 2Re \int d\vec{U} \left\{ \int_0^L dt_2 \int_0^{t_2} dt_1 \cdot \left[\rho\sigma \frac{N_C}{2C_F} f(\vec{U} - x\vec{V}, t_2 - t_1) \right] \left[\rho\sigma \frac{N_C}{2C_F} f_{Born}^*(\vec{U} - x\vec{V}) \right] \right\}_{\omega}^{\omega=\infty}. \quad (3.42)$$

The various terms in (3.42) have simple interpretations. The $\frac{\alpha_s C_F}{\pi^2}$ is the coupling of a gluon to a quark. The $1/L$ comes because we calculate the spectrum per unit length of the medium. The factor $\frac{N_C}{2C_F} f(\vec{U} - x\vec{V}, t_2 - t_1) \rho\sigma dt_1$ is the number of scatterers in the medium, $\rho\sigma dt_1$, times the amplitude with gluon emission at t_1 , evolved in time up to t_2 , the time of emission in the complex conjugate amplitude. The factor $\frac{N_C}{2C_F} f_{Born}^*(\vec{U} - x\vec{V}) \rho\sigma dt_2$ gives the number of scatterers times gluon emission in the complex conjugate Born amplitude. The subtraction of the value of the integrals at $\omega = \infty$ eliminates the medium independent zero-phase contribution. Eq. (3.42) may be simplified using $t \equiv \left(\frac{2C_F}{N_c} \lambda\right) \tau$. Defining $\tau_0 = \frac{N_c}{2C_F} \frac{L}{\lambda}$, we obtain

$$\frac{\omega dI}{d\omega dz} = \frac{\alpha_s N_c}{\pi^2 \lambda} Re \int d\vec{Q} \cdot \left\{ \int_0^{\tau_0} d\tau \left(1 - \frac{\tau}{\tau_0}\right) f(\vec{U} - x\vec{V}, \tau) \cdot f_{Born}^*(\vec{U} - x\vec{V}) \right\}_{\omega}^{\omega=\infty}. \quad (3.43)$$

Due to the specific dependence of f and f_{Born} on \vec{U} and \vec{V} , it is possible to express them in terms of a single impact parameter as :

$$\begin{aligned} f(\vec{U} - x\vec{V}, \tau) &= \int \frac{d\vec{B}}{(2\pi)^2} e^{i\vec{B}\cdot(\vec{U}-x\vec{V})} \tilde{f}(\vec{B}, \tau), \\ f_{Born}(\vec{U} - x\vec{V}) &= \int \frac{d\vec{B}}{(2\pi)^2} e^{i\vec{B}\cdot(\vec{U}-x\vec{V})} \tilde{f}_{Born}(\vec{B}), \end{aligned} \quad (3.44)$$

allowing us to obtain the following expression for the spectrum in impact parameter space :

$$\frac{\omega dI}{d\omega dz} = \frac{\alpha_s N_c}{2\pi^3 \lambda} Re \int \frac{d\vec{B}}{2\pi} \left\{ \int_0^{\tau_0} d\tau \left(1 - \frac{\tau}{\tau_0}\right) \tilde{f}(\vec{B}, \tau) \cdot \tilde{f}_{Born}^*(\vec{B}) \right\}_{\omega}^{\omega=\infty}. \quad (3.45)$$

The generic diagram appears in Figure 3. The complete list of diagrams describing the Born amplitude is shown in Figure 6. Graphs a-c correspond to inelastic reactions with the medium while graphs d-g correspond to forward scattering in the medium. For terms a-c there are corresponding inelastic reactions in the complex conjugate amplitude. In the approximation that the forward elastic amplitude for quark scattering off particles in the medium is purely imaginary, the elastic and inelastic terms are proportional to $V(Q^2)$. The color factors and the expression of each graph contribution are derived in [25].

The quark-gluon amplitude $f(\vec{U}, \vec{V}, t)$ obeys an integral evolution equation derived in [20, 21, 25]. In impact parameter space and in the small- x limit, this equation takes the simple form

$$\frac{\partial}{\partial \tau} \tilde{f}(\vec{B}, \tau) = i\tilde{\kappa} \nabla_B^2 \tilde{f}(\vec{B}, \tau) - 2(1 - \tilde{V}(B))\tilde{f}(\vec{B}, \tau) \quad (3.46)$$

with $\tilde{\kappa} = \frac{2C_F}{N_C} \left(\frac{\lambda\mu^2}{2\omega}\right)$ and $\tilde{f}(\vec{B}, 0) = \tilde{f}_{Born}(\vec{B})$. This equation is a Schrödinger-type evolution equation for the propagation of the quark-gluon system in a QCD medium. Comparing (3.46) to (3.39) is instructive. The term proportional to $\tilde{\kappa}$ in (3.46) is clearly of quantum origin and is associated to the phase of the amplitude

whereas (3.39) is a classical diffusion equation. The contributions entering the expression for the spectrum (3.43) are depicted in Figure 7.

So long as $\tilde{v}(B^2) \equiv 4(1 - \tilde{V}(B)/B^2)$ can be treated as a constant, solving (3.46) proceeds in analogy with that of the 2-dimensional harmonic oscillator with imaginary frequency. We expect that the behavior of $\tilde{v}(B^2)$ is close in general to the Coulomb potential case i.e. $\approx \ell n(1/B^2)$ at small B^2 . The solution of (3.46) to logarithmic accuracy is worked out in [21, 25].

In the case where the (quark) jet is produced in matter, one finds for the gluon spectrum

$$\frac{\omega dI}{d\omega dz} = \frac{2\alpha_s C_F}{\pi L} \left[1 - x + \frac{x^2}{2} \right] \ln |\cos(\omega_0 \tau_0)|, \quad (3.47)$$

from which the energy loss per unit length is derived,

$$-\frac{dE}{dz} = \int_0^\infty \frac{\omega dI}{d\omega dz}, \quad (3.48)$$

i.e.

$$-\frac{dE}{dz} = \frac{\alpha_s N_c}{4} \frac{\mu^2 L}{\lambda} \tilde{v}(\tau_0^{-1}). \quad (3.49)$$

Notice the remarkable relation (cf. Eq. (3.34))

$$-\frac{dE}{dz} = \frac{\alpha_s N_c}{4} p_{\perp W}^2 \quad (3.50)$$

between energy loss and jet p_{\perp} -broadening [24].

4 PATH INTEGRAL APPROACH

This section is devoted to presenting in some detail a different approach to the LPM effect in QCD, based on the so-called light-cone path integral technique for multiple scattering developed in [28]. We refer the reader for derivations and further details to [29] - [34]. Let us give here the essential features of the method

by discussing in scalar QED the formalism for an induced transition $a \rightarrow bc$. The interaction Lagrangian is $L_{int} = \lambda [\hat{\psi}_b^\dagger \hat{\psi}_c^\dagger \hat{\psi}_a + h.c.]$. It is assumed that the decay $a \rightarrow bc$ does not take place in the vacuum. We shall indicate later the proper treatment for realistic QED and QCD.

4.1 Derivation of the basic formulas

The S -matrix element for the $a \rightarrow bc$ transition in an external potential reads

$$\langle bc | \hat{S} | a \rangle = i \int dt d\vec{r} \lambda(z) \psi_b^*(t, \vec{r}) \psi_c^*(t, \vec{r}) \psi_a(t, \vec{r}), \quad (4.51)$$

where ψ_i are the wave-functions, and $\lambda(z)$ adiabatically vanishes at $|z| \rightarrow \infty$.

Let us consider the case of a static external potential. Then we can write ψ_i as

$$\psi_i(t, \vec{r}) = \frac{1}{\sqrt{2E_i}} \exp[-iE_i(t - z)] \phi_i(z, \vec{\rho}), \quad (4.52)$$

where $\vec{\rho}$ is the transverse coordinate, and the function ϕ_i describes the evolution of the ψ_i on the light-cone $t - z = \text{const}$. At high energies $E_i \gg m_i$, after substituting (4.52) into the Klein-Gordon equation, one can obtain for ϕ_i the two-dimensional Schrödinger equation

$$i \frac{\partial \phi_i}{\partial z} = H_i(z) \phi_i, \quad (4.53)$$

$$H_i(z) = -\frac{1}{2\mu_i} \left(\frac{\partial}{\partial \vec{\rho}} \right)^2 + e_i U(\vec{\rho}, z) + \frac{m_i^2}{2\mu_i}, \quad (4.54)$$

where $\mu_i = E_i$, e_i is the electric charge, and U is the potential of the target.

Consequently, the values of the ϕ_i at the $\vec{\rho}$ -planes $z = z_2$ and $z = z_1$ are related by

$$\phi_i(z_2, \vec{\rho}_2) = \int d\vec{\rho}_1 K_i(\vec{\rho}_2, z_2 | \vec{\rho}_1, z_1) \phi_i(z_1, \vec{\rho}_1), \quad (4.55)$$

where $K_i(\vec{\rho}_2, z_2 | \vec{\rho}_1, z_1)$ is the Green function of the Hamiltonian (4.54). Let us introduce the two $\vec{\rho}$ -planes located at large distances in front of ($z = z_i$) and

behind ($z = z_f$) the target. Then, using the convolution relation (4.55) one can express the incoming and outgoing wave-functions in terms of their asymptotic plane-waves at z_i and z_f , respectively. As we shall see below, this representation turns out to be very convenient for the evaluation of the LPM effect. It is one of the key points of the light-cone path integral approach.

The differential cross section can be written as

$$\frac{d^5\sigma}{dx d\vec{q}_b d\vec{q}_c} = \frac{2}{(2\pi)^4} \text{Re} \int d\vec{\rho}_1 d\vec{\rho}_2 \int_{z_1 < z_2} dz_1 dz_2 g F(z_1, \vec{\rho}_1) F^*(z_2, \vec{\rho}_2), \quad (4.56)$$

where $F(z, \vec{\rho}) = \phi_b^*(z, \vec{\rho}) \phi_c^*(z, \vec{\rho}) \phi_a(z, \vec{\rho})$, $\vec{q}_{b,c}$ are the transverse momenta, $x = E_b/E_a$, and $g = \lambda(z_1)\lambda(z_2)/[16\pi x(1-x)E_a^2]$ is the vertex factor. Expressing ϕ_i in terms of the asymptotic plane-waves, (4.56) may be represented diagrammatically by the graph of Figure 8a. We depict $K_i(K_i^*)$ by \rightarrow (\leftarrow). The dotted lines show the transverse density matrix for the initial particle a at $z = z_i$, and the complex conjugate transverse density matrices for the final particles b, c at $z = z_f$. For the spectra integrated over transverse momenta, the relation

$$\int d\vec{\rho}_2 K(\vec{\rho}_2, z_2 | \vec{\rho}_1, z_1) K^*(\vec{\rho}_2, z_2 | \vec{\rho}'_1, z_1) = \delta(\vec{\rho}_1 - \vec{\rho}'_1) \quad (4.57)$$

allows one to transform the graph of Figure 8a into the ones of Figure 8b and Figure 8c for the \vec{q}_c - and $\vec{q}_{b,c}$ -integrated spectra, respectively.

Let us discuss now the $a \rightarrow bc$ transition for a random potential of an amorphous target using the representations of Figure 8. In this case one should perform averaging of the transition cross section over the states of the target. We cannot evaluate analytically the diagrams of Figure 8 for a given state of the target. The basic idea of the approach of [29, 30, 34] is to represent all the propagators in the

path integral form

$$K_i(\vec{\rho}_2, z_2 | \vec{\rho}_1, z_1) = \int D\vec{\rho} \exp \left\{ i \int dz \left[\frac{\mu_i (d\vec{\rho}/dz)^2}{2} - e_i U(\vec{\rho}, z) \right] - \frac{im_i^2(z_2 - z_1)}{2\mu_i} \right\}, \quad (4.58)$$

and to perform averaging over the target states before the integration over the trajectories. It is then remarkable that for the diagrams of Figure 8b,c (and for Figure 8a if b or c has zero charge, say, for the $e \rightarrow \gamma e'$ transition) a considerable part of work on the path integration can be done analytically.

Below we consider the \vec{q}_c -integrated spectrum. Let z_1 and z_2 be the longitudinal coordinates of the left and right vertices of the diagram of Figure 8b. Taking advantage of the convolution relations (we omit the transverse variables) $K_b(z_f | z_1) = K_b(z_f | z_2) \otimes K_b(z_2 | z_1)$, $K_a^*(z_2 | z_i) = K_a^*(z_2 | z_1) \otimes K_a^*(z_1 | z_i)$, we can divide the diagram of Figure 8b into the initial and final state interaction two-body parts (we denote them by S_c and S_b) and the three-body part (we denote it by M) located between them. The factors S_i and M are given in terms of the Green functions (4.58).

Let us first consider the factor S_i : after averaging over the states of the target, the phase factor

$$\exp\{ie_i \int dz [U(\vec{\rho}, z) - U(\vec{\rho}', z)]\} \quad (4.59)$$

can be viewed as the Glauber factor for the $i\bar{i}$ pair. Neglecting the correlations in the positions of the medium constituents one can obtain for the averaged value of this phase factor (we denote it by $\Phi_i(\{\vec{\rho}\}, \{\vec{\rho}'\})$)

$$\Phi_i(\{\vec{\rho}\}, \{\vec{\rho}'\}) = \exp \left[-\frac{1}{2} \int dz \sigma_{i\bar{i}} (|\vec{\rho}(z) - \vec{\rho}'(z)|) n(z) \right], \quad (4.60)$$

where $\{\vec{\rho}\}$ and $\{\vec{\rho}'\}$ are the trajectories for K_i and K_i^* , respectively, $\sigma_{i\bar{i}}$ is the dipole cross section of the interaction with the medium constituent of the $i\bar{i}$ pair,

and $n(z)$ is the number density of the target. Then the S_i is given by the path integral $\int D\vec{\rho}D\vec{\rho}' \exp[i\hat{S}_i(\{\vec{\rho}\}, \{\vec{\rho}'\})]$ with the action

$$\hat{S}_i(\{\vec{\rho}\}, \{\vec{\rho}'\}) = \frac{1}{2} \int dz \{ \mu_i [(d\vec{\rho}/dz)^2 - (d\vec{\rho}'/dz)^2] + i\sigma_{i\bar{i}} (|\vec{\rho}(z) - \vec{\rho}'(z)|) n(z) \}. \quad (4.61)$$

It is important that the interaction term in (4.61) depends only on the relative distance between trajectories. This fact allows one to carry out analytically the path integration and obtain a simple formula [28]

$$S_i(\vec{\rho}_2, \vec{\rho}'_2, z_2 | \vec{\rho}_1, \vec{\rho}'_1, z_1) = K_i^0(\vec{\rho}_2, z_2 | \vec{\rho}_1, z_1) K_i^{0*}(\vec{\rho}'_2, z_2 | \vec{\rho}'_1, z_1) \Phi_i(\{\vec{\rho}_s\}, \{\vec{\rho}'_s\}), \quad (4.62)$$

where

$$K_i^0(\vec{\rho}_2, z_2 | \vec{\rho}_1, z_1) = \frac{\mu_i}{2\pi i(z_2 - z_1)} \exp \left[\frac{i\mu_i(\vec{\rho}_2 - \vec{\rho}_1)^2}{2(z_2 - z_1)} - \frac{im_i^2(z_2 - z_1)}{2\mu_i} \right] \quad (4.63)$$

is the Green function for $U = 0$, $\{\vec{\rho}_s\}$ and $\{\vec{\rho}'_s\}$ denote the straight line trajectories between $\vec{\rho}_{1,2}$ and $\vec{\rho}'_{1,2}$, respectively. Expression (4.62) can be obtained by dividing the z -interval into steps of small width, and taking the multiple integral step by step [28].

The factor M can be treated similarly. The corresponding Glauber factor contains the three-body cross section σ_{abc} depending on the relative transverse separations $\vec{\tau}_{bc} = \vec{\rho}_b - \vec{\rho}_c$ and $\vec{\tau}_{ac} = \vec{\rho}_a - \vec{\rho}_c$ (here and below we view the particle a for a complex conjugate propagator as antiparticle \bar{a}). The path integrals may be performed analytically leading to

$$M(\vec{\rho}_2, \vec{\rho}'_2, z_2 | \vec{\rho}_1, \vec{\rho}'_1, z_1) = K_a^0(\vec{R}_2, z_2 | \vec{R}_1, z_1) K_a^{0*}(\vec{\rho}'_2, z_2 | \vec{\rho}'_1, z_1) K_{bc}(\vec{\rho}_2 - \vec{\rho}'_2, z_2 | 0, z_1), \quad (4.64)$$

where $\vec{R}_1 = \vec{\rho}_1$, $\vec{R}_2 = x\vec{\rho}_2 + (1-x)\vec{\rho}'_2$ are the initial and final coordinates of the centre-of-mass of the bc pair, respectively. The Green function K_{bc} is given by a path integral on $\vec{\tau}_{bc}$ and describes the evolution of the $bc\bar{a}$ system.

Having (4.62) and (4.64), one can represent the spectrum for the $a \rightarrow bc$ transition for the diagram of Figure 8b for $\vec{q}_a = 0$ in the form [34]

$$\begin{aligned} \frac{d^3 I}{dx d\vec{q}_b} &= \frac{2}{(2\pi)^2} \text{Re} \int d\vec{\tau}_b \exp(-i\vec{q}_b \cdot \vec{\tau}_b) \int_{z_i}^{z_f} dz_1 \\ &\cdot \int_{z_1}^{z_f} dz_2 g \Phi_b(\vec{\tau}_b, z_2) K_{bc}(\vec{\tau}_b, z_2 | 0, z_1) \Phi_a(\vec{\tau}_a, z_1), \end{aligned} \quad (4.65)$$

where

$$\begin{aligned} \Phi_a(\vec{\tau}_a, z_1) &= \exp \left[-\frac{\sigma_{a\bar{a}}(\vec{\tau}_a)}{2} \int_{z_i}^{z_1} dz n(z) \right], \\ \Phi_b(\vec{\tau}_b, z_2) &= \exp \left[-\frac{\sigma_{b\bar{b}}(\vec{\tau}_b)}{2} \int_{z_2}^{z_f} dz n(z) \right], \end{aligned} \quad (4.66)$$

are the values of the absorption factors for the parallel trajectories, and $\vec{\tau}_a = x\vec{\tau}_b$. The potential for the Green function K_{bc} entering (4.64) and (4.65) should be evaluated for parallel trajectories of the centre-of-mass of the bc pair and \bar{a} . The resulting Hamiltonian for K_{bc} is given by

$$H_{bc} = -\frac{1}{2\mu_{bc}} \left(\frac{\partial}{\partial \vec{\tau}_{bc}} \right)^2 - \frac{in(z)\sigma_{\bar{a}bc}(\vec{\tau}_{bc}, \vec{\tau}_{\bar{a}c})}{2} + \frac{1}{L_f}, \quad (4.67)$$

where $\mu_{bc} = E_a x(1-x)$ is the reduced Schrödinger mass, $\vec{\tau}_{\bar{a}c} = x\vec{\tau}_{bc} - \vec{\tau}_a$; the formation length is $L_f = 2E_a x(1-x)/[m_b^2(1-x) + m_c^2 x - m_a^2 x(1-x)]$.

For numerical calculations it is convenient to represent (4.65) in another form in which (for a target occupying the region $0 < z < L$) the z -integration is dominated by the region $|z| \leq \max(L_f, L)$. Let us rewrite the integrand of the z_2 -integral in (4.65) as

$$\begin{aligned} &g \{ \Phi_b(\vec{\tau}_b, z_2) [K_{bc}(\vec{\tau}_b, z_2 | 0, z_1) - K_{bc}^0(\vec{\tau}_b, z_2 | 0, z_1)] \Phi_a(\vec{\tau}_a, z_1) \\ &+ [\Phi_b(\vec{\tau}_b, z_2) - 1] K_{bc}^0(\vec{\tau}_b, z_2 | 0, z_1) [\Phi_a(\vec{\tau}_a, z_1) - 1] + K_{bc}^0(\vec{\tau}_b, z_2 | 0, z_1) [\Phi_a(\vec{\tau}_a, z_1) - 1] \\ &+ [\Phi_b(\vec{\tau}_b, z_2) - 1] K_{bc}^0(\vec{\tau}_b, z_2 | 0, z_1) + K_{bc}^0(\vec{\tau}_b, z_2 | 0, z_1) \}. \end{aligned} \quad (4.68)$$

It is evident that in (4.65) the contribution associated with the first two terms of (4.68) will be dominated by the region $|z_{1,2}| \leq \max(L_f, L)$, and can be evaluated neglecting the z -dependence of $\lambda(z)$. However, for the last three terms in (4.68) it is not the case. Taking $z_i = -\infty$, $z_f = \infty$, and using $\lambda(z)$ which exponentially vanishes at $|z| \rightarrow \infty$ one can show that the term $\propto K_{bc}^0$ does not contribute to the spectrum. It is not surprising since this term corresponds to the transition in vacuum. The contribution of the other two terms can be written in terms of the bc Fock component of the light-cone wave-function of the particle a , Ψ_a^{bc} .³

The final expression for the spectrum is given by

$$\begin{aligned}
\frac{d^3 I}{dx d\vec{q}_b} &= \frac{2}{(2\pi)^2} \text{Re} \int d\vec{\tau}_b \exp(-i\vec{q}_b \cdot \vec{\tau}_b) \int_{z_i}^{z_f} dz_1 \int_{z_1}^{z_f} dz_2 \\
&\cdot g \{ \Phi_b(\vec{\tau}_b, z_2) [K_{bc}(\vec{\tau}_b, z_2|0, z_1) - K_{bc}^0(\vec{\tau}_b, z_2|0, z_1)] \Phi_a(\vec{\tau}_a, z_1) \\
&+ [\Phi_b(\vec{\tau}_b, z_2) - 1] K_{bc}^0(\vec{\tau}_b, z_2|0, z_1) [\Phi_a(\vec{\tau}_a, z_1) - 1] \} \\
&- \frac{1}{(2\pi)^2} \int d\vec{\tau} d\vec{\tau}' \exp(-i\vec{q}_b \cdot \vec{\tau}) \Psi_a^{bc*}(x, \vec{\tau}' - \vec{\tau}) \Psi_a^{bc}(x, \vec{\tau}') \\
&\cdot [\Phi_b(\vec{\tau}, z_i) + \Phi_a(x\vec{\tau}, z_f) - 2], \tag{4.69}
\end{aligned}$$

where one can take $z_i = -\infty$, $z_f = \infty$.

Integrating over \vec{q}_b one obtains from (4.69) the x -spectrum

$$\frac{dI}{dx} = 2\text{Re} \int_{z_i}^{z_f} dz_1 \int_{z_1}^{z_f} dz_2 g \left[K_{bc}(\vec{\rho}_2, z_2|\vec{\rho}_1, z_1) - K_{bc}^0(\vec{\rho}_2, z_2|\vec{\rho}_1, z_1) \right] \Big|_{\vec{\rho}_1 = \vec{\rho}_2 = 0}, \tag{4.70}$$

which was derived in [29] using the unitarity connection between the probability of the $a \rightarrow bc$ transition and the radiative correction to the $a \rightarrow a$ transition.

The spectrum (4.70) can be represented in another form demonstrating a close connection between the LPM suppression and Glauber absorption. Treating the

³These terms, which vanish after integrating over \vec{q}_b , have been missed in [34].

second term of the Hamiltonian (4.67) as a perturbation, one obtains

$$\begin{aligned}
K_{bc}(0, z_2|0, z_1) &= K_{bc}^0(0, z_2|0, z_1) + \int_{z_1}^{z_2} d\xi \int d\vec{\rho} K_{bc}^0(0, z_2|\vec{\rho}, \xi)v(\xi, \vec{\rho}) \\
&\cdot K_{bc}^0(\vec{\rho}, \xi|0, z_1) + \int_{z_1}^{z_2} d\xi_1 \int_{\xi_1}^{z_2} d\xi_2 \int d\vec{\rho}_1 d\vec{\rho}_2 K_{bc}^0(0, z_2|\vec{\rho}_2, \xi_2)v(\xi_2, \vec{\rho}_2) \\
&\cdot K_{bc}(\vec{\rho}_2, \xi_2|\vec{\rho}_1, \xi_1)v(\xi_1, \vec{\rho}_1)K_{bc}^0(\vec{\rho}_1, \xi_1|0, z_1), \quad (4.71)
\end{aligned}$$

where $v(z, \vec{\rho}) = -n(z)\sigma_{\bar{a}bc}(\vec{\rho}, x\vec{\rho})/2$. Taking advantage of (4.71) one can represent

(4.70) in the form

$$\frac{dI}{dx} = \frac{dI^{BH}}{dx} + \frac{dI^{abs}}{dx}, \quad (4.72)$$

$$\frac{dI^{BH}}{dx} = T \int d\vec{\rho} |\Psi_a^{bc}(x, \vec{\rho})|^2 \sigma_{\bar{a}bc}(\vec{\rho}, x\vec{\rho}), \quad (4.73)$$

$$\frac{dI^{abs}}{dx} = -\frac{1}{2} \text{Re} \int_0^L dz_1 n(z_1) \int_{z_1}^L dz_2 n(z_2) \int d\vec{\rho} \Psi_a^{bc*}(x, \vec{\rho}) \sigma_{\bar{a}bc}(\vec{\rho}, x\vec{\rho}) \Phi(x, \vec{\rho}, z_1, z_2), \quad (4.74)$$

where $T = \int_0^L dz n(z)$ [30], and

$$\Phi(x, \vec{\rho}, z_1, z_2) = \int d\vec{\rho}' K_{bc}(\vec{\rho}, z_2|\vec{\rho}', z_1) \Psi_a^{bc}(x, \vec{\rho}') \sigma_{\bar{a}bc}(\vec{\rho}', x\vec{\rho}') \quad (4.75)$$

is the solution of the Schrödinger equation with the boundary condition

$$\Phi(x, \vec{\rho}, z_1, z_1) = \Psi_a^{bc}(x, \vec{\rho}) \sigma_{\bar{a}bc}(\vec{\rho}, x\vec{\rho}). \quad (4.76)$$

The first term in (4.72) corresponds to the impulse approximation. It dominates the cross section in the low-density limit (the Bethe-Heitler regime). The second term describes absorption effects responsible for the LPM suppression.

For a sufficiently thin target the absorptive correction (4.74) can be evaluated neglecting the transverse motion in the $\bar{a}bc$ system inside the target (it corresponds to neglecting the kinetic term in (4.67)). Then, the Green function takes a simple eikonal form

$$K_{bc}(\vec{\rho}_2, z_2|\vec{\rho}_1, z_1) \approx \delta(\vec{\rho}_2 - \vec{\rho}_1) \exp \left[-\frac{\sigma_{\bar{a}bc}(\vec{\rho}_1, x\vec{\rho}_1)}{2} \int_{z_1}^{z_2} dz n(z) \right], \quad (4.77)$$

and (4.72)-(4.74) give

$$\frac{dI^{fr}}{dx} = 2 \int d\vec{\rho} |\Psi_a^{bc}(x, \vec{\rho})|^2 \Gamma_{abc}^{eik}(\vec{\rho}, x\vec{\rho}), \quad (4.78)$$

with $\Gamma_{abc}^{eik}(\vec{\tau}_{bc}, \vec{\tau}_{ac}) = \{1 - \exp[-T\sigma_{abc}(\vec{\tau}_{bc}, \vec{\tau}_{ac})/2]\}$. This is the ‘‘frozen-size’’ approximation corresponding to the factorization regime discussed in section 3.

The above analysis is performed for the particle a incident on a target from outside. If it is produced in a hard reaction inside a medium one should replace in equations (4.65), (4.69) and (4.70) z_i by the coordinate of the production point, and in (4.69) the factor $[\Phi_a - 1]$ should be replaced by Φ_a . Note that due to the infinite time required for the formation of a light-cone wave-function Ψ_a^{bc} , (4.72) does not hold in this case.

4.2 Generalization to the realistic QED Lagrangian

The generalization of the above analysis to the realistic QED and QCD Lagrangian is simple. Let us consider first the $e \rightarrow e'\gamma$ transition in QED. The \hat{S} -matrix element can be obtained by replacing in (4.51) λ by $e\bar{u}_{e'}\gamma^\nu\epsilon_\nu u_e$ where ϵ_ν is the photon polarization vector, and $u_{e'}, u_e$ are the electron spinors in which the transverse momenta should be regarded as operators acting on the corresponding wave-functions. Since the photon does not interact with the target, one has $\sigma_{\bar{e}\gamma e'}(\vec{\tau}_{\gamma e'}, \vec{\tau}_{\bar{e}e'}) = \sigma(|\vec{\tau}_{\bar{e}e'}|)$, where σ is the dipole cross section for the e^+e^- pair. In terms of the electron-atom differential cross section it reads

$$\sigma(\vec{\rho}) = \frac{2}{\pi} \int d\vec{q} [1 - \exp(i\vec{q} \cdot \vec{\rho})] \frac{d\sigma}{dq^2}. \quad (4.79)$$

The dipole cross section vanishes as $\vec{\rho} \rightarrow 0$, and one can write it as $\sigma(\vec{\rho}) = C(\rho)\vec{\rho}^2$, where $C(\rho)$ has a smooth logarithmic dependence at small $\vec{\rho}$ [28, 36].

In the Bethe-Heitler regime the radiation rate is dominated by $\tau_{\bar{e}e'} < 1/m_e$; for

the case of strong LPM suppression the typical values of $\tau_{\bar{e}e'}$ are even smaller. One can approximate the Hamiltonian (4.67) by the harmonic oscillator Hamiltonian, and obtain from (4.70) the radiation rate per unit length. In an infinite medium, in the regime of strong LPM suppression, the radiation rate per unit length takes the form

$$\frac{dI}{dx dz} \approx \frac{\alpha[4 - 4x + 2x^2]}{2\pi} \sqrt{\frac{C(\rho_{eff}x)}{2x(1-x)E_e}}. \quad (4.80)$$

The value of ρ_{eff} can be estimated as $\rho_{eff} \sim (2L'_f/\mu_{\gamma e'})^{1/2}$ where the formation length L'_f is the typical value of $|z_2 - z_1|$ in (4.70). One can see that for strong suppression ρ_{eff} becomes much smaller than $1/m_e x$, the characteristic transverse size in the Bethe-Heitler regime. For this reason the spectrum for strong suppression (4.80) is insensitive to the electron mass [35]. Note that the oscillator approximation is equivalent to the Fokker-Planck approximation in momentum representation used in Migdal's analysis [2]. This fact is not surprising since within logarithmic accuracy $\sigma(\rho) \propto \vec{\rho}^2$ leads to a Gaussian diffusion of the electron in transverse momentum space [28]. This feature underlies the relationship given in section 3 relating the energy loss and p_{\perp} -broadening in QCD.

For an accurate numerical evaluation of the LPM effect it is convenient to use the form given by (4.72)-(4.74). In [30, 33] it is used for the analysis of the recent data on bremsstrahlung from high energy electrons taken by the E-146 SLAC collaboration [3]. Excellent agreement (at the level of the radiative corrections) with the data is found.

4.3 Induced gluon emission in QCD

Let us now discuss the induced gluon emission from a fast quark in QCD. At the level of the radiation cross section, involving the sum over states of the medium,

one can formulate the theory similarly to the case of QED. The path integral representations for the diagrams of Figure 8 can be written by introducing into the vacuum path integral formulas the Glauber factors for propagation of the color neutral partonic systems (consisting of the partons from the amplitude and complex conjugate one). The quark trajectory for the complex conjugate amplitude can be regarded as that of an antiquark with negative kinetic and mass terms. It follows from the relation $-T_q^* = T_{\bar{q}}$ (here $T_{q,\bar{q}}$ are the color generators for a quark and an antiquark). The $q\bar{q}$, gg , $q\bar{q}g$ configurations which can appear in the graphs like those of Figure 8b,c, have only one color singlet state, and the diffraction operator has only diagonal matrix elements involving the two-body cross sections $\sigma_{q\bar{q}}(\vec{\rho}), \sigma_{gg}(\vec{\rho}) = \frac{9}{4}\sigma_{q\bar{q}}(\vec{\rho})$, and the three-body one $\sigma_{gq\bar{q}}(\vec{\rho}_{gq}, \vec{\rho}_{\bar{q}q}) = \frac{9}{8}[\sigma_{q\bar{q}}(|\vec{\rho}_{gq}|) + \sigma_{q\bar{q}}(|\vec{\rho}_{\bar{q}q}|)] - \frac{1}{8}\sigma_{q\bar{q}}(|\vec{\rho}_{q\bar{q}}|)$ [36]. Thus, the spectra integrated over quark or/and gluon transverse momenta can be evaluated similarly to the above case of the $a \rightarrow bc$ transition in QED, with all the particles now being charged.

For the x -spectrum (4.70) $\vec{\rho}_{\bar{q}q} = x\vec{\rho}_{gq}$, and the three-body cross section takes the form $\sigma_{gq\bar{q}}(\vec{\rho}_{gq}, x\vec{\rho}_{gq}) = \frac{9}{8}[\sigma_{q\bar{q}}(\rho) + \sigma_{q\bar{q}}((1-x)\rho)] - \frac{1}{8}\sigma_{q\bar{q}}(x\rho)$, where $\rho = |\vec{\rho}_{gq}|$. Similarly to QED, one can estimate the spectrum using the oscillator parametrization $\sigma_{gq\bar{q}}(\vec{\rho}, x\vec{\rho}) \approx C_3(x)\vec{\rho}^2$, where $C_3(x) = \frac{1}{8}\{9[1 + (1-x)^2] - x^2\}C_2(\rho_{eff})$, $C_2(\rho_{eff}) = \sigma_{q\bar{q}}(\rho_{eff})/\rho_{eff}^2$. Here ρ_{eff} is the typical size of the $q\bar{q}g$ system dominating the radiation rate, which in the limit of strong LPM suppression takes the form

$$\frac{dI}{dx dz} \approx \frac{\alpha_s(4 - 4x + 2x^2)}{3\pi} \sqrt{\frac{2nC_3(x)}{E_q x^3(1-x)}}. \quad (4.81)$$

Ignoring the contributions to the energy loss from the two narrow regions near $x \approx 0$ and $x \approx 1$, in which (4.81) is not valid, one finds the energy loss per unit

length

$$\frac{d\Delta E_q}{dz} \approx 1.1\alpha_s \sqrt{nC_3(0)E_q}, \quad (4.82)$$

where to logarithmic accuracy $\rho_{eff} \sim [\alpha_s^2 n E_q x(1-x)]^{-1/4}$ is taken. Note that as in QED, the elimination of the infrared divergence for strong suppression is a direct consequence of the medium modification of the gluon formation length which makes the typical transverse distances much smaller than $1/m_{g,q}$.

The medium modification of the formation length plays an important role in the case of gluon emission by a quark produced inside a medium. In this case the finite-size effects become important and suppress the radiation rate (cf. (3.47)). This finite-size suppression leads to the L^2 dependence of the quark energy loss for a high energy quark (3.49). One obtains

$$\Delta E_q \sim \alpha_s C_3(0) n L^2. \quad (4.83)$$

This regime takes place as long as $L \leq (E_q/nC_3(0))^{1/2}$. Then it transforms into the $\Delta E_q \propto L$ behavior given by (4.82). More detailed discussions and numerical estimates are given in [31, 32]. The $g \rightarrow gg$ transition can be evaluated in an analogous way. The ggg system can be in antisymmetric (F) and symmetric (D) color states. However, the two-gluon Pomeron exchanges do not generate the $F \leftrightarrow D$ transitions. This allows one to express the emission probability through the Green function for F state.

4.4 Comparison with the BDMPS approach

We conclude this section with a comment on the connection between the path integral approach with the approach discussed in section 3.

Let us consider the case of a parton entering the medium from outside. The equivalence of the two approaches may be established using (4.72)-(4.74) together

with (4.78), in the zero mass case as assumed in BDMPS [21]. As it was mentioned, the "frozen-size" expression (4.78) corresponds to the factorization contribution, neglected in the BDMPS approach, on the ground of its weak medium dependence. Rewriting (4.72) as

$$\frac{dI}{dx} = \frac{dI^{abs}}{dx} + \frac{dI^{fr}}{dx} - \left(\frac{dI^{fr}}{dx} - \frac{dI^{BH}}{dx} \right), \quad (4.84)$$

and ignoring the second term, one can show that

$$\frac{dI}{dx} = \frac{dI^{abs}}{dx} \Big|_{\omega=\infty}^{\omega}, \quad (4.85)$$

together with identifying in (4.74) the product $\Psi_a^{bc} \sigma_{\bar{a}bc}$ and Φ with the amplitudes f_{Born} and f , respectively, which are discussed in section 3.

For the case of a parton produced inside a medium, say at $z = 0$, in (4.70) $z_i = 0$, one should subtract from the right hand side of (4.72) the contribution corresponding to the configurations with $z_1 < 0$ and $z_2 > 0$ in (4.70). The additional term corresponds to the additional contribution in the BDMPS approach due to the hard scattering in the medium. In this case the "frozen-size" expression is medium independent and it may be obtained by taking the limit of dI^{abs}/dx when $\omega \rightarrow \infty$. Further details concerning this comparison can be found in [25].

5 RADIATIVE ENERGY LOSS IN AN EXPANDING QCD PLASMA

In the previous sections we have discussed the suppression of gluon radiation due to multiple scatterings of energetic partons propagating through dense matter with properties constant in time.

Here we consider the case of a parton, of high energy E , traversing an expanding

hot QCD medium. We concentrate on the induced gluon radiation, the resulting energy loss of a quark, and its relation to jet broadening [37, 38].

Let us imagine the medium to be a quark-gluon plasma produced in a relativistic central AA collision, which occurs at (proper) time $t = 0$. We have in mind the realistic situation where the quark is produced by a hard scattering in the (not yet thermalized) medium, and at time t_0 it enters the homogeneous plasma at high temperature T_0 , which expands longitudinally with respect to the collision axis. Consider t_0 to be the thermalization time, and for most of the results the limit $t_0 \rightarrow 0$ may be taken with impunity. The quark, for simplicity, is assumed to propagate in the transverse direction with vanishing longitudinal momentum, i.e. at rapidity $y = 0$, such that its energy is equal to its transverse momentum. On its way through the plasma the quark hits layers of matter which are cooled down due to the longitudinal expansion. It is assumed that the plasma lives long enough so that the quark is able to propagate on a given distance L within the quark-gluon phase of matter.

As a consequence of the medium expansion the parton propagation in the transverse direction, z , is affected by the position-dependent density of the plasma $\rho(z)$ and the parton cross section $d\sigma/d^2\vec{q}_\perp(\vec{q}_\perp, z)$. Therefore the screening mass μ and the mean free path λ depend on z . When the properties of the expanding plasma are described by the hydrodynamical model proposed by Bjorken [39], one has the scaling law

$$T^3 t^\alpha = \text{const}, \quad (5.86)$$

where the (proper) time t at rapidity $y = 0$ coincides with the distance z on which the quark has propagated through the plasma. The power α , approximated in the following by a constant, may take values between 0 and 1 for an ideal fluid.

Correspondingly, the transport coefficient $\hat{q}(t)$ defined as

$$\hat{q}(t) \simeq \rho(t) \int d^2\vec{q}_\perp \vec{q}_\perp^2 \frac{d\sigma}{d^2\vec{q}_\perp} = \frac{\mu^2(t)}{\lambda(t)} \tilde{v} \quad (5.87)$$

becomes time-dependent and satisfies

$$\hat{q}(t) = \hat{q}(t_0) \left(\frac{t_0}{t} \right)^\alpha, \quad (5.88)$$

due to (5.86).

As a result [37] the radiative energy loss ΔE for the quark (produced in the medium) traversing an expanding medium is

$$-\Delta E = \frac{2}{2-\alpha} \frac{\alpha_s N_c}{4} \hat{q}(L) L^2. \quad (5.89)$$

In the high temperature phase of QCD matter [10]

$$1 - \alpha = O(\alpha_s^2(T)). \quad (5.90)$$

The coefficient $\hat{q}(L) = \hat{q}(T(L))$ has to be evaluated at the temperature $T(L)$ the quark finally “feels” after having passed the distance L through the medium, which during this propagation cools down to $T(L)$. One may, however, notice that the limit $\alpha = 1$ for an expanding ideal relativistic plasma can be taken. In this limit the maximal loss is achieved. It is bigger by a factor 2 than the corresponding static case at fixed temperature $T(L)$.

So far we have discussed the result for the case for $E > E_{cr}(L)$, actually taking $E \rightarrow \infty$. In [38] the approach of the quark’s energy loss ΔE to this limit is studied numerically as a function of the quark energy E . For instance, with $L = 6$ fm, one finds (almost) energy independence on E , when $E > 100$ GeV $\simeq E_{cr}$, as given by (5.89).

In summary one expects indeed that the energy loss in an expanding medium be larger than in the static case taken at the final temperature, since the parton

passes through hotter layers during the early phase of the expansion. Perhaps the surprising feature is that there is no dependence of the enhancement factor on the initial temperature T_0 . This result has to be associated to the coherence pattern of the medium induced radiation. Gluons contributing to the energy loss require finite time for their emission, and therefore effects of the early stages of the quark-gluon plasma expansion are reduced.

6 INDUCED ENERGY LOSS OF A HARD QUARK JET IN A FINITE CONE

Let us consider a typical calorimetric measurement of hard jets produced in heavy ion collisions [40]. The consequence of a large energy loss is the attenuation of the spectrum usually denoted as jet quenching. It is necessary to study the angular distribution of radiated gluons in order to give quantitative predictions for the energy lost by a jet traversing hot matter. Only the gluons which are radiated outside the cone defining the jet contribute to the energy loss.

In [34, 41, 42] the calculation of the angular distribution is discussed for a hard jet produced in the medium. Here we have in mind a hard quark jet of high energy E produced by a hard scattering in a dense QCD medium and propagating through it over a distance L . Following [41] we concentrate on the integrated loss *outside* an angular cone of opening angle θ_{cone} (Figure 9),

$$-\Delta E(\theta_{\text{cone}}) = L \int_0^\infty d\omega \int_{\theta_{\text{cone}}}^\pi \frac{\omega dI}{d\omega dz d\theta} d\theta. \quad (6.91)$$

In the following we consider the normalized loss by defining the ratio

$$R(\theta_{\text{cone}}) = \frac{\Delta E(\theta_{\text{cone}})}{\Delta E}. \quad (6.92)$$

This ratio $R(\theta_{\text{cone}})$ turns out to depend on one single dimensionless variable

$$R = R(c(L)\theta_{\text{cone}}), \quad (6.93)$$

where

$$c^2(L) = \frac{N_c}{2C_F} \hat{q} (L/2)^3. \quad (6.94)$$

The “scaling behaviour” of R means that the medium and size dependence is universally contained in the function $c(L)$, which is a function of the transport coefficient \hat{q} and of the length L , as defined by (6.94). In Figure 10, we show the variation of R with θ_{cone} . The ratio $R(\theta_{\text{cone}})$ is also universal in the sense that it is the same for an energetic quark as well as for a gluon jet. The fact that θ_{cone} scales as $1/c(L)$ may be understood from the following physical argument [22]: the radiative energy loss of a quark jet is dominated by gluons having $\omega \simeq \hat{q}L^2$. The angle that the emitted gluon makes with the quark is $\theta \simeq k_{\perp}/\omega$, and $k_{\perp}^2 \simeq \hat{q}L$ so that the typical gluon angle will be $\theta^2 \simeq 1/\hat{q}L^3$.

So far we have discussed the *medium-induced* energy loss. Concerning the total energy loss of a jet of a given cone size it is important to take into account the *medium independent* part, which for a quark jet in a cone may be estimated [41],

$$-\Delta E^{\text{fact}}(\theta_{\text{cone}}) \simeq \frac{4}{3} \frac{\alpha_s C_F}{\pi} E \ln \left(\frac{\theta_{\text{max}}}{\theta_{\text{cone}}} \right), \quad (6.95)$$

using a constant α_s (θ_{max} is taken $\mathcal{O}(\pi/2)$).

7 PHENOMENOLOGICAL IMPLICATIONS

The parameter controlling the magnitude of the energy loss is \hat{q} . Estimates can be provided for its value, allowing us to give orders of magnitude for the radiative induced energy loss. The following numbers are estimates for a quark jet produced in matter.

For hot matter taking $T = 250$ MeV, $\frac{\mu^2}{\lambda} \sim 1$ GeV/fm² taken from perturbative estimates at finite T , a typical value for $\tilde{v} \approx 2.5$, we find $\hat{q} \simeq 0.1$ GeV³ [24]. With $\alpha_s = \frac{1}{3}$, this leads for the total induced energy loss to

$$-\Delta E \approx 60 \text{ GeV} \left(\frac{L}{10 \text{ fm}} \right)^2 . \quad (7.96)$$

In [24] it is shown that for cold nuclear matter it is possible to relate \hat{q} to the gluon structure function G evaluated at an average scale $\mu^2 \frac{\lambda}{L}$, actually

$$\hat{q} \simeq \frac{2\pi^2 \alpha_s}{3} \rho [xG(x)]. \quad (7.97)$$

Taking the nuclear density $\rho \sim 0.16$ fm⁻³, $\alpha_s = \frac{1}{2}$, $xG \sim 1$ for $x < 0.1$, it is found that

$$-\Delta E \approx 4 \text{ GeV} \left(\frac{L}{10 \text{ fm}} \right)^2 . \quad (7.98)$$

These values do suggest that hot matter may be effective in stimulating significant radiative energy loss of high energy partons. As discussed in section 5 the energy loss is larger in an expanding hot medium than in the corresponding static one.

Next we turn to the medium-induced $-\Delta E(\theta_{\text{cone}})$ for energetic jets. We may use the estimates above to give orders of magnitude for $c(L)$ in the case of a hot/cold medium :

$$c(L)_{\text{hot}} \simeq 40 (L/10 \text{ fm})^{3/2} .$$

A much smaller value is found in the cold nuclear matter case :

$$c(L)_{\text{cold}} \sim 10 (L/10 \text{ fm})^{3/2} .$$

As expected from the fact that $R(\theta_{\text{cone}})$ depends universally on $c(L)\theta_{\text{cone}}$, Figure 10 shows that the jets are more collimated in the hot medium than in the cold one. The loss is, however, still appreciably large even for cone sizes of order $\theta_{\text{cone}} \simeq 30^\circ$.

Again, keeping in mind that the estimates are based on the leading logarithm approximation, we show in Figure 11 the variation of $\Delta E(\theta_{cone})$ with θ_{cone} of the medium-induced (for a hot medium with $T = 250$ MeV) and the medium independent energy losses.

Let us now give a few representative examples of phenomena sensitive to parton energy loss in dense matter. Available experimental results are, it seems, essentially instructive for future measurements at higher energies.

As a projectile traverses dense nuclear matter the width of the transverse momentum distribution of partons may increase. pA and AA scattering allow to study parton p_{\perp} -broadening of initial quarks in the Drell-Yan process of lepton pair production, and of gluons in J/Ψ production, respectively (see e.g. [43, 44]). Recently, the analysis of J/Ψ data shows indeed p_{\perp} -broadening of the intrinsic gluon distribution, which when translated into the ratio \hat{q}/ρ results into $\hat{q}/\rho = 9.4 \pm 0.7$ [45]. Neglecting final state effects this should be compared with $\hat{q}/\rho \sim 7.4 [xG(x)]$.

The above quoted processes also contain information on the energy loss in the initial state due to matter effects [46, 47]. In the Drell-Yan process the observed energy loss $-\Delta E$ of the incident quarks is indeed compatible with the estimate given in (7.98), including the L^2 dependence, as measured and analysed in [48].

Large p_{\perp} particle and jet spectra and production rates in high-energy collisions are especially sensitive to a finite energy loss, when the partons are propagating through long-lived high density media before hadronization. Under extreme conditions the jets may even be "extincted" [7]. However, hadron spectra from present experiments of pp, pA and AA collisions, mainly from CERN-SPS, do not show any strong evidence of suppression [49, 50]. This observation which is

obscured by large theoretical uncertainties may indicate that at present energies the life time of the dense partonic matter may be shorter than the mean free path of the propagating partons. Significant jet quenching should become clearly observable in AA collisions at RHIC and higher energies, even for transverse momenta as low as $p_{\perp} \geq 3$ GeV: the magnitude of the predicted jet quenching is commented upon in [51, 52]. Suppression of hadronic p_{\perp} distributions in the case of a thin plasma, therefore due to only a small number (≤ 3) of scatterings, is analysed in [53].

Jet quenching for very high energy jets is also discussed in [40, 54, 55]. In particular the ratio of monojet versus dijets observed in ultra-relativistic heavy ion collisions is predicted.

A further interesting proposal to study the modification of jet fragmentation due to energy loss is proposed in [56, 57]. Noting that photons are essentially not affected by hadronic media, the conjecture is to measure the charged particle p_{\perp} distribution in the opposite transverse direction of a tagged photon, i.e. in $\gamma + \text{jet}$ events of high energy heavy ion collisions. With increased luminosity this may be even possible at RHIC energies.

Valuable and important information about dense hadronic matter produced in collisions is provided by dileptons, either from Drell-Yan processes or from final heavy meson decays [58]. In this context Shuryak [59] pointed out the importance of the energy loss of charm (bottom) quarks due to their interactions in the medium. In the extreme case they may be even stopped in dense matter. Assuming e.g. that the charmed mesons D and D^* take all the charm quark momentum in the fragmentation process the final leptons from the semileptonic decay populate the invariant dilepton mass spectrum at masses below $1 - 2$ GeV

(4 – 5 GeV from bottom decays): as a result dilepton spectra in AA collisions for invariant masses above 2 GeV are not dominated by correlated semileptonic charm and bottom decays. This expected strong suppression due to energy loss is confirmed in further detailed (Monte Carlo) studies in [60, 61, 62].

8 OUTLOOK

In this review we have described the more recent results related to energy loss and p_{\perp} -broadening of a high energy quark or gluon (jet) traversing QCD media. Phenomenological implications for measurements in cold as well in hot (QGP) matter have been discussed. The orders of magnitude found for the energy lost by an energetic jet in hot deconfined matter indicate the interest of the corresponding measurements as specific signals.

A couple of important open questions triggered by the coherent character of the induced energy loss remain open. One is related to the formulation of a transport model (Monte Carlo) which correctly simulates the interference pattern of gluon radiation induced by multiple scattering [18, 22]. It is indeed crucial when calculating rates for processes leading to thermal and chemical equilibration of partons to include medium effects [63] - [69]. In the same context let us mention the influence of the LPM effect on the production of dileptons and real photons produced in a QGP, or in a hadron gas [70]. In any case the partons are not very energetic, since their energies are of the order of the plasma temperature. This forbids to use the asymptotic treatment discussed in the above.

We already mentioned that the above discussed numerical estimates give only orders of magnitude in particular since they are obtained in leading order in the QCD coupling. The main aim of the present investigations is therefore to encour-

age experimentalists at RHIC, and later at LHC, to carefully explore heavy quark production and especially jet phenomena in ultra-relativistic heavy ion collisions [71]. High p_{\perp} nuclear physics may become an exciting new frontier at these colliders [52], because of the possible jet "extinction" or crucial modifications of the spectra [7]. The best guiding example comes from the long-term study of hard jets in hadron-hadron scattering, starting from the first evidence at the CERN-ISR until the analysis of jet cross sections up to transverse momenta of $p_{\perp} \simeq 500$ GeV at CDF and DØ, which has been successfully carried out within an active interplay between experiments and perturbative QCD [72].

Medium effects will continue to attract increasing attention, and we hope that finally the described suppression mechanism will be demonstrated by future experiments in a convincing manner. More detailed treatments and improvements are certainly necessary in view of completing this program. It constitutes an important chapter of what has been recently designated [73] as the "health report" of QCD.

9 ACKNOWLEDGEMENTS

R. B. and D. S. are grateful for the pleasant and fruitful collaboration with Yu. L. Dokshitzer, A. H. Mueller and S. Peigné on the different aspects of these topics during the last few years. We thank M. Dirks, I. P. Lokhtin, D. Denegri, K. Redlich, H. Satz, E. Shuryak and A. Smilga for valuable comments and discussions. Partial support by DFG under contract Ka 1198/4-1 is acknowledged.

Literature Cited

1. Landau LD, Pomeranchuk IY. *Dokl. Akad. Nauk SSSR* 92:535, 735 (1953)
2. Migdal AB. *Phys. Rev.* 103:1811 (1956)

3. Anthony PL, et al (E-146 SLAC Collaboration). *Phys. Rev. Lett.* 75:1949 (1995); *Phys. Rev.* D56:1373 (1997)
4. Klein S. *Rev. Mod. Phys.* 71:1501 (1999)
5. Jackson JD. *Classical Electrodynamics* (John Wiley & Sons, New York 1975) p.618
6. Ter-Mikaelian ML. *High Energy Electromagnetic Processes in Condensed Media* (John Wiley & Sons, New York, 1972)
7. Bjorken JD. Fermilab publication Pub-82/59-THY, Batavia (1982), Erratum, unpublished
8. Thoma MH. *Quark-Gluon Plasma 2* ed. Hwa RC. (World Scientific, Singapore, 1995) p.51
9. LeBellac M. *Thermal Field Theory* (Cambridge University Press, Cambridge, 1996)
10. For a recent review, see: Nieto A. *Int. Journal of Modern Phys.* A12:1431 (1997)
11. Braaten E, Pisarski RD. *Phys. Rev. Lett.* 64:1338 (1990); Braaten E, Pisarski RD. *Nucl. Phys.* B337:569 (1990); B399:310 (1990)
12. Frenkel J, Taylor JC. *Nucl. Phys.* B334:199 (1990)
13. Braaten E, Thoma MH. *Phys. Rev.* D44:R2625 (1991)
14. Thoma MH. *Phys. Lett.* B273:128 (1991)
15. Mustafa MG, Pal D, Srivastava DK. *Phys. Rev.* C57:889 (1998)
16. Baier R, Dirks M, Redlich K. hep-ph/9910353 (1999)
17. Casher A, Neuberger H, Nussinov S. *Phys. Rev.* D20:179 (1979); Kopeliovich BZ, Niedermayer F. *Yad. Fiz.* 42:797 (1985)
18. Gyulassy M, Wang XN. *Nucl. Phys.* B420:583 (1994)
19. Wang XN, Gyulassy M, Plümer M. *Phys. Rev.* D51:3436 (1995)
20. Baier R, Dokshitzer YL, Peigné S, Schiff D. *Phys. Lett.* B345:277 (1995)
21. Baier R, Dokshitzer YL, Mueller AH, Peigné S, Schiff D. *Nucl. Phys.* B483:291(1997)
22. Dokshitzer YL. *Nucl. Phys.* A638:291c (1998)
23. Gunion JF, Bertsch G. *Phys. Rev.* D25:746 (1982)
24. Baier R, Dokshitzer YL, Mueller AH, Peigné S, Schiff D. *Nucl. Phys.* B484:265 (1997)
25. Baier R, Dokshitzer YL, Mueller AH, Schiff D. *Nucl. Phys.* B531:403 (1998)
26. Knoll J, Voskresensky DN. *Ann. Phys.* 249:532 (1996)
27. Kovchegov YV, Mueller AH. *Nucl. Phys.* B529:451 (1998)
28. Zakharov BG. *Sov. J. Nucl. Phys.* 46:92 (1987)

29. Zakharov BG. *JETP Lett.* 63:952 (1996)
30. Zakharov BG. *JETP Lett.* 64:781 (1996)
31. Zakharov BG. *JETP Lett.* 65:615 (1997)
32. Zakharov BG. *Phys. Atom. Nucl.* 61:838 (1998)
33. Zakharov BG. *Phys. Atom. Nucl.* 62:1008 (1999)
34. Zakharov BG. *JETP Lett.* 70:176 (1999); hep-ph/9906373 (1999)
35. Baier R, Dokshitzer YL, Mueller AH, Peigné S, Schiff D. *Nucl. Phys.* B478:577(1996)
36. Nikolaev NN, Zakharov BG. *JETP* 78:598 (1994)
37. Baier R, Dokshitzer YL, Mueller AH, Schiff D. *Phys. Rev.* C58:1706 (1998)
38. Zakharov BG. hep-ph/9807396 (1998)
39. Bjorken JD. *Phys. Rev.* D27:140 (1983)
40. Lokhtin IP, Snigirev AM. *Phys. Lett.* B440:163 (1998)
41. Baier R, Dokshitzer YL, Mueller AH, Schiff D. *Phys. Rev.* C60:064902 (1999)
42. Wiedemann UA, Gyulassy M. *Nucl. Phys.* B560:345 (1999)
43. Gavin S, Gyulassy M. *Phys. Lett.* B214:241 (1988)
44. Hüfner J, Kurihara Y, Pirner HJ. *Phys. Lett.* B215:218 (1988)
45. Kharzeev D, Nardi M, Satz H. *Phys. Lett.* B405:14 (1997)
46. Brodsky JS, Hoyer P. *Phys. Lett.* B298:165 (1993)
47. Nagle JL, Bennett MJ. *Phys. Lett.* B465:21 (1999)
48. Vasiliev MA, et al (FNAL E866/NuSea Collaboration). *Phys. Rev. Lett.* 83:2304 (1999)
49. Wang XN. *Prog. Theor.Phys. Suppl.* 129:45 (1997)
50. Wang XN. *Phys. Rev. Lett.* 81:2655 (1998); *Phys. Rev.* C58:2321 (1998)
51. Gyulassy M, Levai P. *Phys. Lett.* B442:1 (1998)
52. Gyulassy M. *Last call for RHIC predictions* eds. Bass S, et al. nucl-th/9907090
53. Gyulassy M, Levai P, Vitev I. hep-ph/9907343; hep-ph/9907461
54. Lokhtin IP. hep-ph/9904418 (1999)
55. Lokhtin IP, Sarychera LI, Snigirev AM. hep-ph/9906369 (1999)
56. Wang XN, Huang Z, Sarcevic I. *Phys. Rev. Lett.* 77:231 (1996)
57. Wang XN, Huang Z. *Phys. Rev.* C55:3047 (1997)
58. McGaughey PL, Moss JM, Peng JC. *Ann. Rev. Nucl. Part. Sci.* to appear; hep-ph/9905409

59. Shuryak E. *Phys. Rev.* C55:961 (1997)
60. Lin Z, Vogt R, Wang XN. *Phys. Rev.* C57:899 (1998)
61. Lin Z, Vogt R. *Nucl. Phys.* B544:339 (1999)
62. Gallmeister K, Kämpfer B, Pavlenko OP. *Phys. Rev.* C57:3276 (1998); *Prog. Part. Nucl. Phys.* 42:335 (1999)
63. Biro TS, van Doorn E, Müller B, Thoma MH, Wang XN. *Phys. Rev.* C48:1275 (1993)
64. Geiger K. *Phys. Rev.* D56:2665 (1997)
65. Wang XN. *Phys. Rep.* 280:287 (1997)
66. Wong SMH. *Phys. Rev.* C54:2588 (1996); C56:1075 (1997)
67. Srivastava DK. *Nucl. Phys.* A647:136 (1999)
68. Müller B. nucl-th/9902065
69. Eskola KJ. hep-ph/9911350 (1999)
70. Cleymans J, Goloviznin VV, Redlich K. *Quark-Gluon Plasma 2* ed. Hwa RC. (World Scientific, Singapore, 1995) p.454
71. Harris JW, Müller B. *Ann. Rev. Nucl. Part. Sci.* 46:71 (1996)
72. Sterman G, et al. *Rev. Mod. Phys.* 67:157 (1995)
73. Dokshitzer Y. *Proc. of 29th ICHEP* eds. Astbury A, et al. (World Scientific, Singapore, 1999) 1:305 (1999)

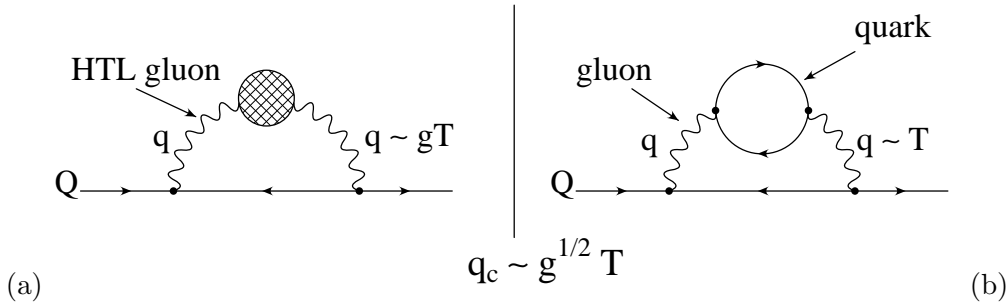


Figure 1: Self-energy diagrams contributing to the collisional energy loss: (a) in HTL-resummed perturbation theory for soft exchanged momentum and (b) in fixed leading order for hard exchanged momentum.

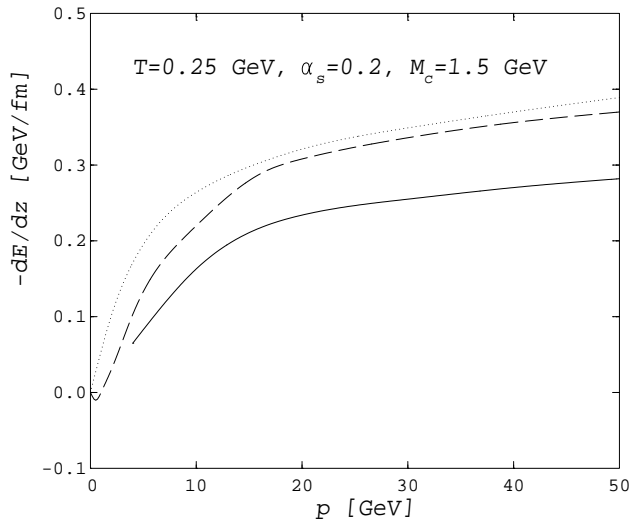


Figure 2: Collisional energy loss of a charm quark as a function of its momentum. The quark propagates through an out-of-chemical equilibrium plasma with fugacities $\lambda_g = 1, \lambda_q = 0$ (solid curve) [16]. The dashed curve is the equilibrium result of [13], the dotted curve shows the original prediction by Bjorken [7].

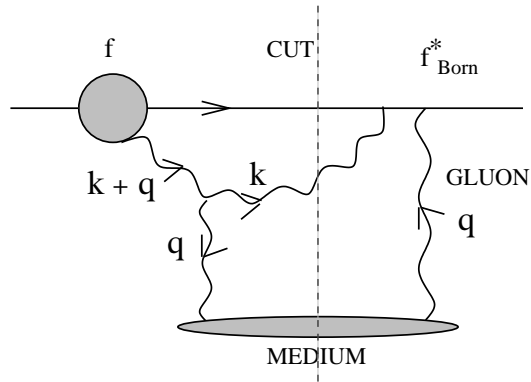


Figure 3: Contribution to the induced gluon spectrum by interference between the amplitude f and the Born amplitude f_{Born} .

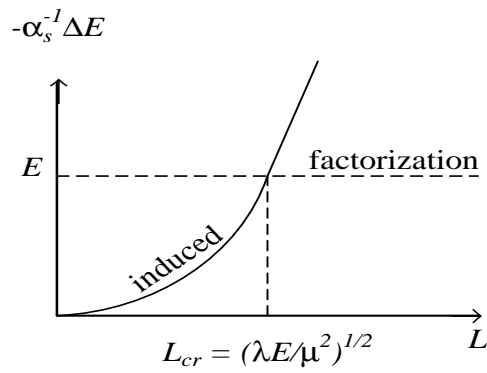


Figure 4: Energy loss as a function of the medium size L .

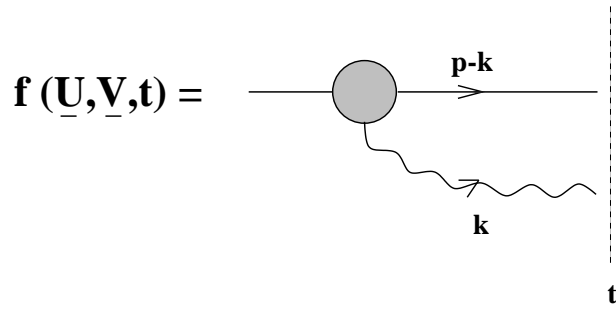
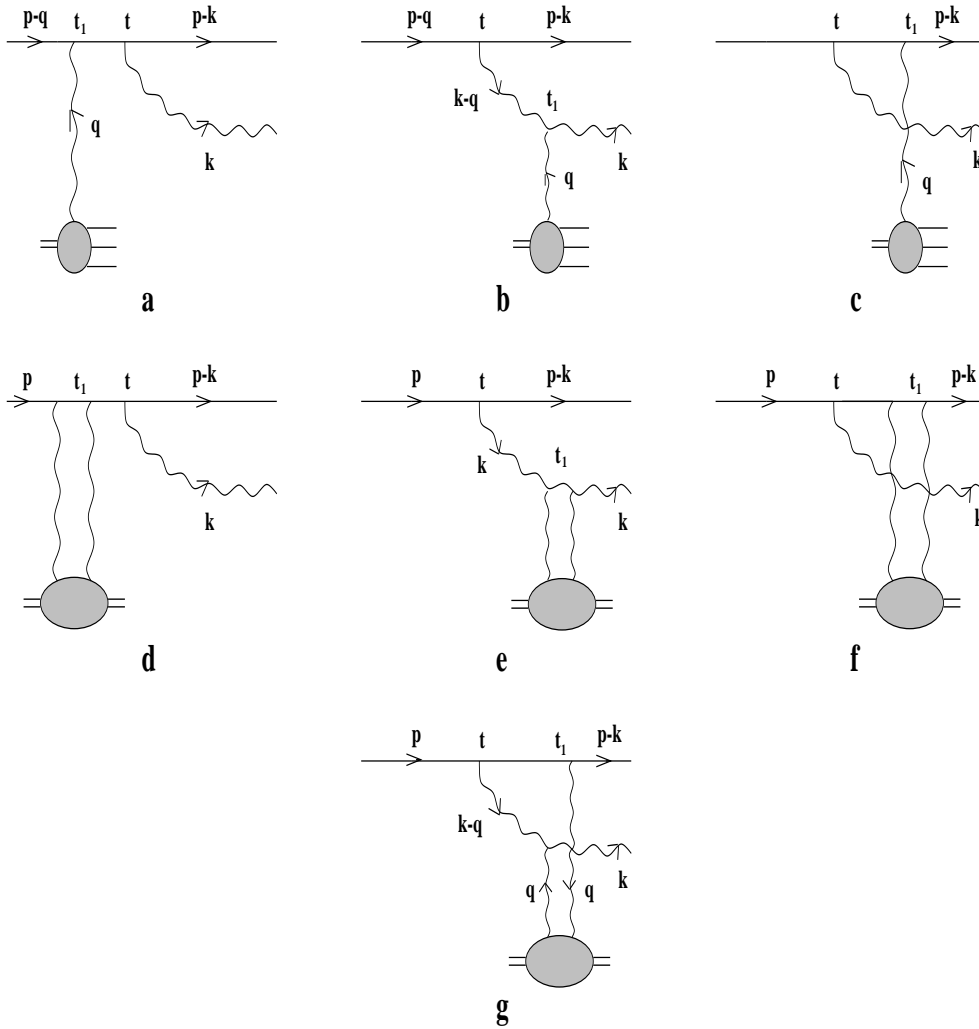
Figure 5: Quark gluon amplitude at time t .

Figure 6: The diagrams representing the Born terms for the amplitude.

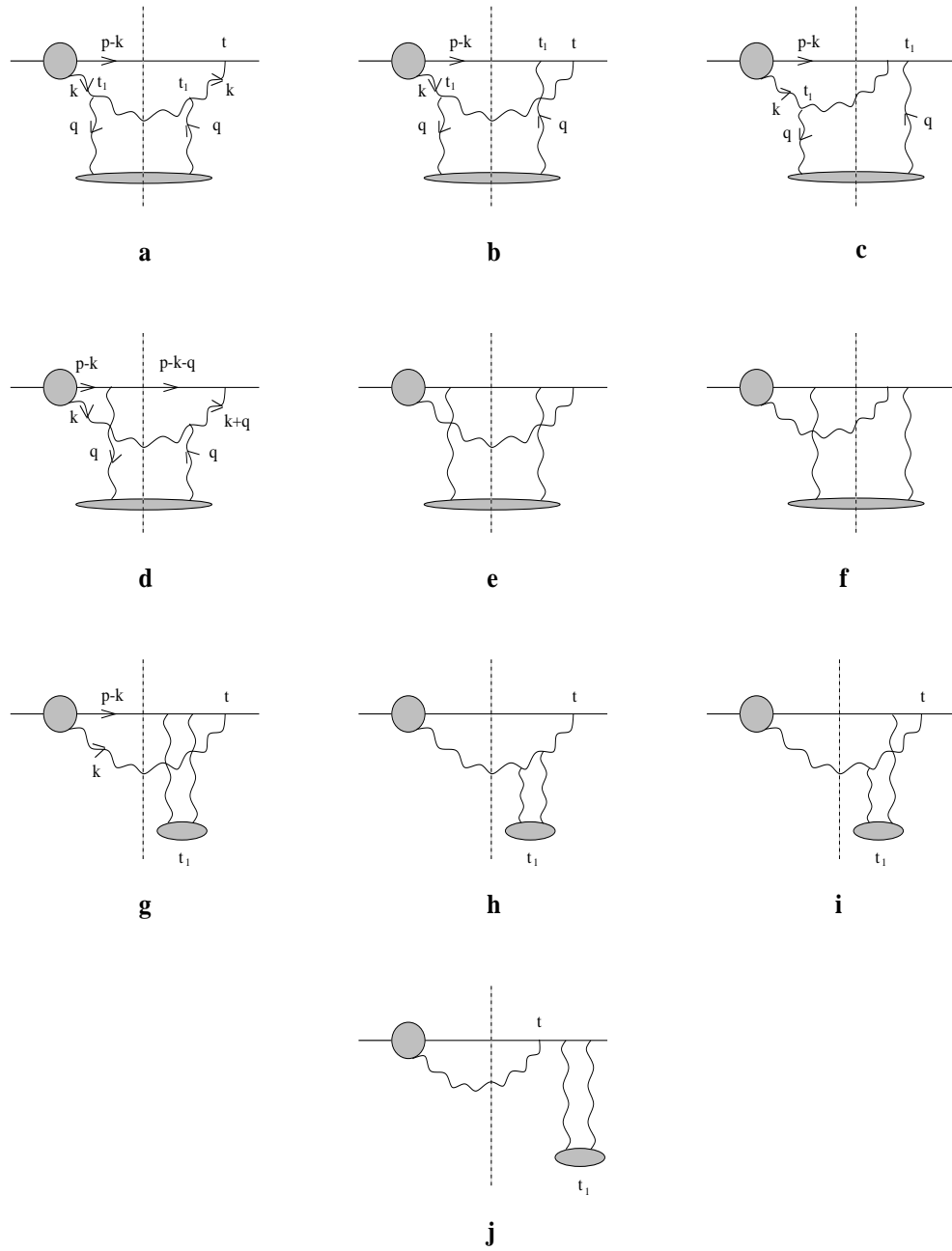


Figure 7: Graphs describing the gluon emission.

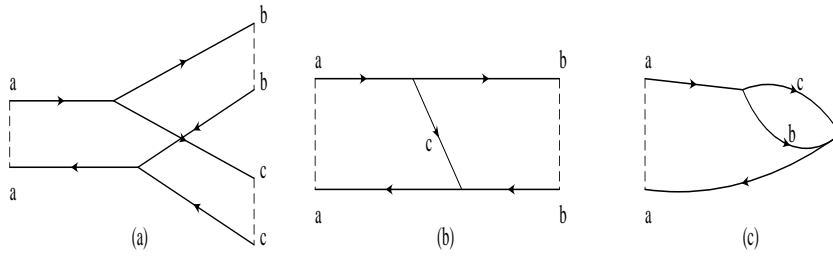


Figure 8: Diagrammatic representation of the $a \rightarrow bc$ transition in terms of the two-dimensional Green functions.

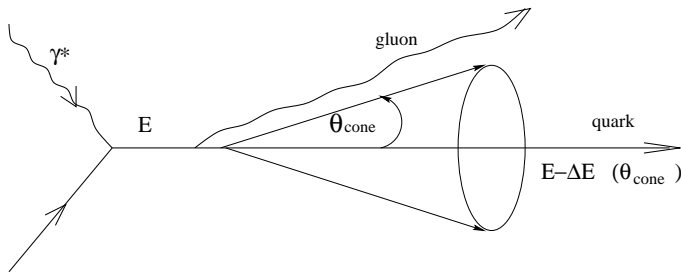


Figure 9: Example of a hard process producing a quark jet. The gluon is emitted outside the cone with angle θ_{cone} .

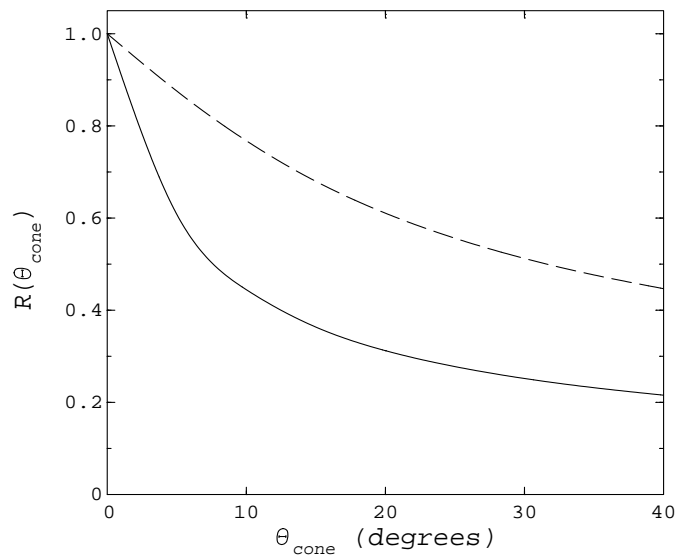


Figure 10: Medium induced (normalized) energy loss distribution as a function of cone angle θ_{cone} for hot ($T = 250$ MeV) (solid curve) and cold matter (dashed curve) at fixed length $L = 10$ fm.

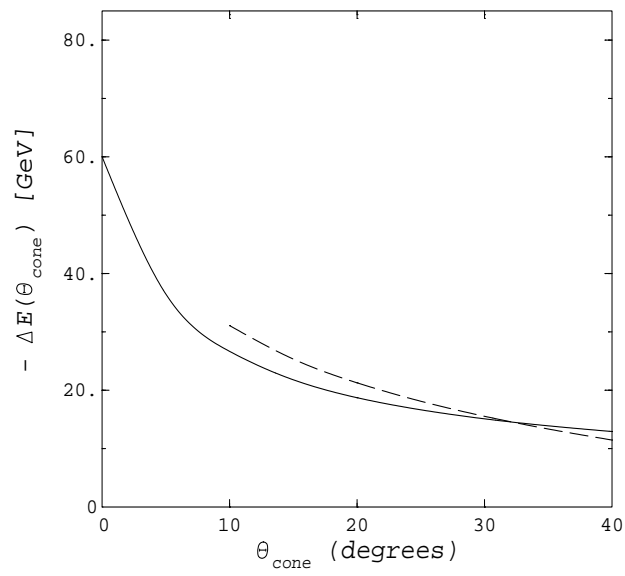


Figure 11: Energy loss in a hot medium, $T = 250$ MeV, as a function of θ_{cone} .

The dashed curve represents the medium independent piece for $E = 250$ GeV.

$L = 10$ fm.